

Four-dimensional imaging of thoracic target volumes in conformal radiotherapy



Edward M. Leter

Four-dimensional imaging of thoracic target volumes in conformal radiotherapy

Several chapters of this thesis are based on published papers, which are reproduced with permission of the publishers. Copyright of these papers remains with the publishers.

ISBN 90-8559-022-1

Cover: R.P. Slagter

Printed by: Optima, Rotterdam

□ 2005, E.M. Leter

Four-dimensional imaging of thoracic target volumes in conformal radiotherapy

**Vierdimensionale beeldvorming van thoracale doelvolumina
in de conformatieradiotherapie**

PROEFSCHRIFT

ter verkrijging van de graad van doctor aan de
Erasmus Universiteit Rotterdam
op gezag van de
Rector Magnificus

Prof. dr. S.W.J. Lamberts

en volgens besluit van het College voor Promoties.

De openbare verdediging zal plaatsvinden op
woensdag 5 januari 2005 om 11:45 uur

door

Edward Martin Leter
geboren te Haarlem

Promotiecommissie

Promotor: Prof. dr. P.C. Levendag

Overige leden: Prof. dr. P.M.T. Pattynama
Prof. dr. P.W. Serruys
Prof. dr. E.P. Krenning

Copromotor: Dr. P.J.C.M. Nowak

This thesis has been prepared at the department of Radiation Oncology of the Erasmus MC, Rotterdam, The Netherlands.

Financial support by the Hendrika Stichting for the publication of this thesis is gratefully acknowledged.

Voor mijn ouders

Contents

Chapter 1	Introduction	9
Chapter 2	Coronary stent traversed volume during the cardiac cycle defined as a target for high-precision radiotherapy by using biplane angiograms	15
Chapter 3	A biplane angiographic study on cardiac motion of coronary artery stents: Options to minimize the target volume for high-precision external beam radiotherapy of coronary artery in-stent restenosis	25
Chapter 4	Definition of a moving gross target volume for stereotactic radiation therapy of stented coronary arteries	37
Chapter 5	Dosimetric comparison between high-precision external beam radiotherapy and endovascular brachytherapy for coronary artery in-stent restenosis	49
Chapter 6	Three-dimensional lung tumor displacements throughout consecutive respiratory cycles determined by multislice spiral computed tomography	63
Chapter 7	Four-dimensional multislice spiral computed tomography for determination of respiratory lung tumor motion in conformal radiotherapy	71
Chapter 8	Summary and conclusions	81
	Samenvatting en conclusies	87
	Dankwoord	93
	List of publications	95
	Curriculum vitae	97

Chapter

1

Introduction

The goal of conformal radiotherapy (CRT) is to deliver the prescribed dose to a volume that closely conforms to the three-dimensional (3D) target volume while the dose to adjacent healthy tissues or organs at risk is minimized. Because the position of the target volume can change substantially both within and between radiation treatment fractions the fourth dimension, namely time, needs to be addressed as well. The consideration of time in the 3D treatment process is referred to as four-dimensional (4D) radiotherapy. Variations in the target volume position with time are mainly due to organ motion and patient and beam set-up deviations. Changes in the target volume position that occur within a treatment fraction are referred to as intra-fraction variation. Respiratory and cardiac motion are the main contributors to intra-fraction positional variations of thoracic and abdominal target volumes.

In routine clinical practice thoracic and abdominal tumors are irradiated while the patient breathes freely. To account for target volume variations in size, shape and position and patient and beam set-up deviations, an empirical 3D margin is added to the clinical target volume to obtain the planning target volume (1, 2). The 3D margin is often derived from respiratory motion measurements in patients representative of the general population. Such a margin is not tailored to the individual patient and will therefore be suboptimal in most cases. Alternatively, the tumor motion in a specific patient can be determined as part of the treatment planning procedure. Fluoroscopy is most widely used for this purpose. However, tumors are often poorly visualized using this imaging modality. In addition, fluoroscopic data cannot directly be related to the treatment planning computed tomography (CT) data.

Recently, several strategies to reduce the impact of respiratory motion have been explored. Two distinct techniques have been used: either the patient is allowed to breathe freely or not. In the case of free breathing techniques, irradiation can be gated to a part of the respiratory cycle where tumor motion is minimal (3), or the moving target can be tracked by the continuous radiation beam (4). Both strategies have the potential to improve the therapeutic ratio, but require challenging imaging and respiratory monitoring efforts that will also pose a substantial demand on departmental logistics. The second technique is based on voluntary (5) or forced breath hold strategies (6). These breath holding techniques may also improve the therapeutic ratio, but likewise demand challenging technical efforts. Many lung cancer patients may have difficulties to tolerate repeated breath holds. In addition, because the radiation fraction needs to be delivered in small portions, the treatment duration will substantially increase. The latter drawback also applies for gated treatment, but not for tumor tracking CRT.

Next to respiratory motion, the other main contributor to thoracic and upper abdominal intra-fraction target volume movement is cardiac motion. Ekberg *et*

al. (7) studied lung tumor movement in 20 patients by fluoroscopy and found significant cardiac motion of tumors situated close to the heart. Ross *et al.* (8) studied intrathoracic neoplasm movement in 20 patients by an ultra-fast CT scanner. Five out of six hilar lesions showed significant lateral motion with cardiac contraction. These studies did not qualitatively separate respiratory from cardiac tumor motion. Seppenwoolde *et al.* (9) on the other hand did separate between these motion effects. They studied the 3D motion of markers implanted in or near lung neoplasms using a real-time tumor tracking system consisting of two fluoroscopy image processor units. They detected cardiac tumor motion in seven out of the 20 studied patients. The amplitude of this motion was 1–4 mm, mostly in the lateral direction.

This thesis describes the development of strategies to account for respiratory and cardiac motion for each patient individually in CRT. State-of-the-art imaging techniques have been used for this purpose. Embedded in the general aim of the thesis, strategies to determine and incorporate cardiac motion in the target volume have been explored by studying the clinical feasibility of CRT for the treatment of coronary artery in-stent restenosis, as an alternative to intravascular brachytherapy. The results of the studies to define coronary artery stents as a potential target volume are described in chapters 2 to 5. Chapter 2 describes how coronary artery stent motion during the cardiac cycle can be determined by biplane angiography for definition of a potential CRT target volume. Chapter 3 reports on a comparison of different options to define a smallest feasible potential target volume for external beam radiation treatment of coronary artery stents using angiographic data. Chapter 4 describes how multislice spiral computed tomography (MSCT) can be used to determine and incorporate cardiac motion of coronary artery stents for definition of a potential CRT target volume. Chapter 5 reports the results of a treatment planning study for such a MSCT-defined target volume. Chapters 6 and 7 deal with strategies to determine and account for respiratory lung tumor motion in CRT. Chapter 6 describes how respiratory motion of such tumors can be determined by MSCT. Chapter 7 reports on a comparison between a 3D and a 4D MSCT imaging strategy to account for respiratory lung tumor motion.

References

1. ICRU. Prescribing, recording and reporting photon beam therapy. ICRU Report 50. Washington, 1993.
2. ICRU. Prescribing, recording and reporting photon beam therapy. ICRU Report 62. Washington, 1999.
3. Kubo HD, Len PM, Minohara S, *et al.* Breathing-synchronized radiotherapy program at the University of California Davis Cancer Center. *Med Phys* 2000;27:346-353.
4. Shirato H, Shimizu S, Kitamura K, *et al.* Four-dimensional treatment planning and fluoroscopic real-time tumor tracking radiotherapy for moving tumor. *Int J Radiat Oncol Biol Phys* 2000;48:435-442.
5. Rosenzweig KE, Hanley J, Mah D, *et al.* The deep inspiration breath-hold technique in the treatment of inoperable non-small-cell lung cancer. *Int J Radiat Oncol Biol Phys* 2000;48:81-87.
6. Wong JW, Sharpe MB, Jaffray DA, *et al.* The use of active breathing control (ABC) to reduce margin for breathing motion. *Int J Radiat Oncol Biol Phys* 1999;44:911-919.
7. Ekberg L, Holmberg O, Wittgren L, *et al.* What margins should be added to the clinical target volume in radiotherapy treatment planning for lung cancer? *Radiother Oncol* 1998;48:71-77.
8. Ross CS, Hussey DH, Pennington EC, *et al.* Analysis of movement of intrathoracic neoplasms using ultrafast computerized tomography. *Int J Radiat Oncol Biol Phys* 1990;18:671-677.
9. Seppenwoolde Y, Shirato H, Kitamura K, *et al.* Precise and real-time measurement of 3D tumor motion in lung due to breathing and heartbeat, measured during radiotherapy. *Int J Radiat Oncol Biol Phys* 2002;53:822-834.

Chapter

2

Coronary stent traversed volume during the cardiac cycle defined as a target for high-precision radiotherapy by using biplane angiograms

Edward M. Leter
Johan C.H. Schuurbiens
Peter C. Levendag
Peter J.C.M. Nowak
Jolanda J. Wentzel
Stéphane G. Carlier
Patrick W. Serruys
Pim J. de Feijter
Cornelis J. Slager

Radiother Oncol 2002;63:103–106

Abstract

Three-dimensional reconstructions of 19 coronary artery stents from biplane angiograms were used for measurement of the volume through which the stents traversed during the cardiac cycle. This volume, less than 0.8% of the whole heart volume in all patients, represents a target volume for high-precision radiotherapy to treat coronary artery in-stent restenosis.

Introduction

Several randomized clinical trials have demonstrated that intracoronary γ - and β -radiation, as an adjunct modality to angioplasty, are potent new therapies for coronary artery in-stent restenosis (4,12). Nevertheless, intracoronary brachytherapy suffers from several radiobiological, clinical, physical and logistic disadvantages that may be addressed by the use of external beam radiotherapy (EBRT). Its noninvasive nature, improved dose homogeneity over a range of tissue depths, flexibility to optimize the time of treatment in relation to target cell proliferation following percutaneous transluminal coronary angioplasty, dose fractionation and use of radiosensitizers are examples of the advantages EBRT offers over intracoronary brachytherapy. However, animal studies on the effects of EBRT – targeted at virtually the entire heart – for inhibition of coronary artery restenosis reported conflicting results, and also without exception reported cardiac tissue side effects (5,8,11). Although these animal studies include a recent report that a single, high dose of 21 Gy EBRT targeted at the whole heart can significantly inhibit coronary artery in-stent restenosis (11), clinical implementation of such a treatment may only be feasible when side effects are prevented. Hence high-precision EBRT has been suggested as a strategy to explore (2,5,6,11). The purpose of this study was to use three-dimensional (3D) reconstructions of coronary artery stents from biplane angiograms for measurement of the volume through which the stents traversed during the cardiac cycle in an attempt to define a target volume for high-precision EBRT to treat coronary artery in-stent restenosis.

Materials and methods

Patients

Nineteen coronary artery Wallstents (Schneider, Bülach, Switzerland) in 19 patients (14 men, five women; mean age 58 ± 9 years; mean weight 82 ± 11 kg) in sinus rhythm who underwent conventional angiography were studied. The stented arteries included the left circumflex (LCx; $n = 3$), the left anterior descending (LAD; $n = 7$) and the right coronary artery (RCA; $n = 9$). The mean stent diameter was 3.8 ± 0.6 mm, and the mean stent length was 29.9 ± 10.9 mm. The University Hospital Ethical Review Board approved the study, and informed consent was obtained from all participants.

Acquisition and processing of X-ray images

Biplane X-ray filming (BICOR, Siemens, Forchheim, Germany) during a breathhold was performed at 25 frames per second (0.04-s temporal resolution). For calibration of the X-ray geometrical settings, a calibration cube (axis length 40 mm) and a flat calibration grid were filmed after the procedure. Films and the simultaneously recorded electrocardiogram (ECG) were stored in DICOM format (8 bits, 512 x 512 pixels) on a compact disk. From the film recordings, biplane sets of contrast-free frames clearly showing the stent and covering at least one R-R interval of the cardiac cycle were selected and stored on a personal computer. Consequently, the number of selected sets of frames was dependent on the heart rate. The borders of the stent were contoured manually in the selected sets of frames. For contour determination, custom-made software was used, incorporating standard zooming and contrast optimization features to aid recognition of image details. In the calibration images, the edges of the calibration cube and a 5 x 5-cm area of the grid were indicated.

Three-dimensional reconstruction

The method to 3D reconstruct coronary artery stents uses the algorithm previously described to 3D reconstruct the centerline of an intravascular ultrasound catheter (10). The centerline of the stent in each biplane view was derived from the stent contours. By using these centerlines the 3D centerline can be reconstructed. On the 3D centerline 64 equidistant points were defined. At each point a circle was constructed perpendicular to the centerline assuming a circular cross section. The diameter of the circles was derived from the mean 2D stent diameter in both views corrected for the local magnification factors. Accuracy of the spatial reconstruction of the centerline was determined by the root mean square (RMS) of the distances between the 2D projections of the 64 equidistant points of the 3D reconstructed centerline and corresponding points in the actual drawings.

Data analysis

The length of the reconstructed centerline, i.e. the stent length, was measured in 3D as the cumulative distance between the 64 points along the reconstructed centerline. Three-dimensional displacement of the proximal and distal stent ends throughout the R-R interval of the cardiac cycle was measured relative to the firstly defined end-diastolic location (R peak). By using the latter measurements, the accuracy by which the stent returned to the same location at the end of the R-R interval was calculated (Figure 1).

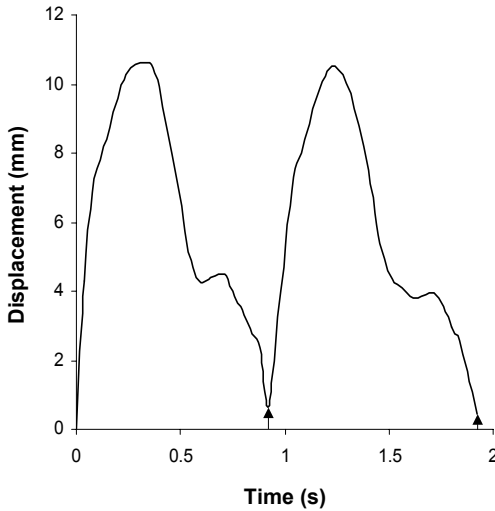


Figure 1. Graph showing an example of the three-dimensional displacement of a left anterior descending coronary artery stent (proximal end) throughout the cardiac cycle. The arrow depicts the accuracy by which the stent returned to the same location at the end of the R-R interval for two successive cardiac cycles; this spatial distance has no specifically defined direction.

The stent volume was calculated from the stent length and the mean diameter. By defining 32, equidistant, points on each stent circular cross section, a total of 2048 (64×32) stent surface points were obtained. The stent traversed volume (STV) during the R-R interval of the cardiac cycle was determined by mapping the 2048 surface points of each stent reconstruction to corresponding cubes (0.5 mm) in a 3D voxel space. Also, the gaps between successive stent reconstructions were mapped to 3D by connecting all corresponding surface points with a spline interpolation algorithm. In addition, all voxels enclosed inside the stent surface map were detected by a fill algorithm and added to the STV. The sum of all mapped voxel cubes represented the STV. To demonstrate the accuracy of the reconstruction and STV algorithm, a straight stainless-steel tube with a diameter of 4.0 mm and a length of 25.3 mm was filmed when moving along a straight path over a distance of 34.7 mm. The stent volume and STV were 0.3 cm^3 and 3.8 cm^3 , respectively.

An estimate of the whole heart volume (WHV) was calculated by the equations as have been reported by Erikson *et al.* (1).

Statistical analysis

All values are expressed as mean \pm SD. One-way analysis of variance followed by the Dunnett's post hoc test was used to compare the means of the maximum stent end displacements, stent volumes, stent traversed volumes and WHV estimates for the three stented coronary artery groups, i.e. the LCx, LAD and RCA. Linear

regression analysis was used to test the relationship between the STV and stent volume for LAD and RCA stents within the range of data points. The Student's *t*-test was used to test the difference between the slopes of the two regression lines. A value of $P < 0.05$ was considered significant.

Results

The average RMS distance between the biplane back-projected 3D reconstructed stent centerlines and the actual 2D centerlines was less than 0.5 mm for each patient (mean 0.37 ± 0.08 mm).

The accuracy by which the stent returned to the same location at the end of the R-R interval of the cardiac cycle was 1.5 ± 1.4 mm for the proximal stent end and 1.6 ± 1.6 mm for the distal stent end. For 10 patients with stents in the LCx ($n = 3$), LAD ($n = 3$) and RCA ($n = 4$), data of two successive cardiac cycles was investigated. The accuracy by which the proximal and distal stent end returned to the same location at the end of the first R-R interval was 1.7 ± 1.3 mm and 1.4 ± 1.3 mm, respectively, and 1.6 ± 1.0 mm and 1.6 ± 1.4 mm at the end of the second R-R interval, respectively.

The mean maximum displacement of the proximal stent end during the R-R interval of the cardiac cycle for the LCx, LAD and RCA, respectively, was 12.8 ± 4.4 , 8.7 ± 1.3 and 24.6 ± 4.9 mm ($P < 0.001$); the mean maximum displacement of the RCA was significantly higher than that of the LCx ($P = 0.044$) and LAD ($P < 0.001$). The mean maximum displacement of the distal stent end during the R-R interval of the cardiac cycle for the LCx, LAD and RCA, respectively, was 13.9 ± 0.6 , 8.6 ± 1.4 and 19.3 ± 7.9 mm ($P = 0.006$); the mean maximum displacement of the LAD significantly differed from that of the LCx ($P < 0.001$) and RCA ($P = 0.009$).

The measured stent volume and STV, as derived from the stainless-steel tube, was 0.3 and 3.9 cm³, respectively, which corresponded to a relative error of -5.8% and $+3.7\%$, respectively. For the LCx, LAD and RCA, the mean stent volume was 0.26 ± 0.01 , 0.28 ± 0.12 and 0.44 ± 0.19 cm³, respectively ($P = 0.094$). The mean STV was 2.3 ± 0.6 , 1.5 ± 0.4 and 5.7 ± 2.7 cm³ for the LCx, LAD and RCA, respectively ($P = 0.001$); the mean STV of the RCA was significantly higher than that of the LCx ($P = 0.014$) and LAD ($P = 0.005$). Linear regression analysis was used to evaluate the relationship between the STV and stent volume for the LAD and RCA data points (Figure 2). The slope of the regression line was significantly higher ($P = 0.01$) for the RCA (STV = $12.84 (\pm 6.22) \times$ stent volume + $0.04 (\pm 2.94)$; $r^2 = 0.85$; $P < 0.001$) than for the LAD (STV = $2.25 (\pm 2.97) \times$ stent volume + 0.88

(± 0.89); $r^2 = 0.44$; $P = 0.73$), i.e. corresponding stent volumes result in higher stent traversed volumes during the cardiac cycle in the case of RCA compared to LAD stents. No regression line was drawn for the LCx, because only three data points were available.

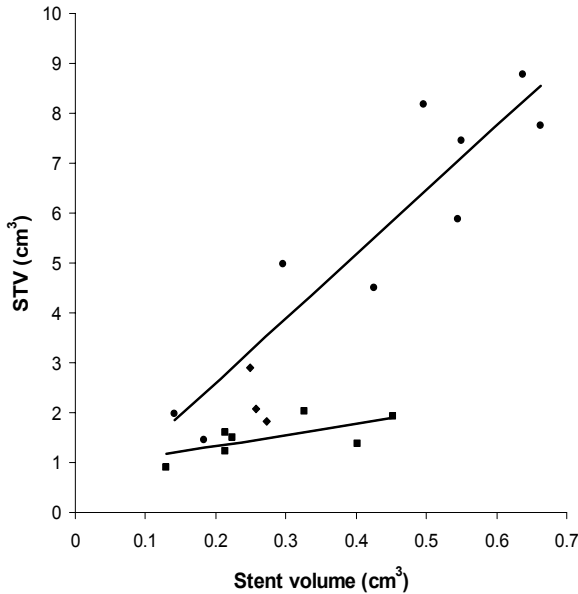


Figure 2. Scatter diagram showing the relationship between the stent traversed volume (STV) and stent volume. \blacklozenge , left circumflex; \blacksquare , left anterior descending; \bullet , right coronary artery.

The stent traversed volumes were also related to estimates of the WHV. The mean estimated WHV was 1226 ± 225 cm³. The STV represented less than 0.8% of the WHV in all patients. There was no significant difference between the means of the WHV estimates for the LCx, LAD and RCA ($P = 0.214$).

Discussion

The present study demonstrates that 3D reconstruction of coronary artery stents from biplane angiograms allowed measurement of the STV. This volume, a combined measure of the stent size and cardiac motion effect during the cardiac cycle, represented less than 0.8% of the whole heart volume in all patients. The definition of the STV represents a successful attempt to define a target volume for high-precision EBRT to treat coronary artery in-stent restenosis.

The observed relationship between the STV and stent volume, i.e. corresponding stent volumes result in higher stent traversed volumes during the cardiac cycle in the case of RCA compared to LAD stents (Figure 2), concurs with the calculated differences between the mean maximum displacements of the LAD and RCA and previous reports on cardiac motion of coronary arteries (7,13). Although based on a limited number of data points, the results probably reflect the different anatomic courses and different orientation of the LAD versus the RCA with respect to the main direction of cardiac motion. As opposed to the LAD, the stented segments of the RCA run through the atrioventricular sulcus in the basal plane of the heart. Since cardiac motion increases from apex to base (7,9), the RCA stents will show greater motion. In addition, the anatomic course of the RCA has an almost perpendicular orientation to the main direction of cardiac motion, i.e. from basal plane to apex (9), while the LAD has a more parallel orientation to the main direction of cardiac motion, which may also partially explain our observations.

Because of its superior image quality and temporal resolution, biplane X-ray angiography allows measurement of the STV, however it does not provide imaging data compatible with EBRT treatment planning software. An additional computed tomography (CT) scan would need to be performed to address this problem. To allow clinical implementation in high-precision EBRT treatment planning, the CT scan and angiographic films, of both the patient and calibration cube, would need to be performed by using the same high-precision coordinate system. The position of the patient and calibration cube during the CT scan would then need to be exactly reproduced during X-ray angiography. The stereotactic body frame (SBF) can be used for this purpose. The SBF is essentially a box with shallow sides and an open top in which the patient lies, held firmly in a vacuum pillow. It provides a coordinate system external to the patient's body and thereby enables noninvasive, accurate and reproducible patient immobilization for stereotactic diagnostic localization and radiotherapy (3,14).

The fact that respiratory motion was not yet accounted for is a limitation of this study. This subject warrants a future study to establish a precise and reproducible internal target volume. Also only one, particularly radio-opaque, type of coronary artery stent was studied.

In conclusion, the results demonstrate that 3D reconstruction from biplane angiograms of stents in the three major epicardial coronary arteries allows the definition of a target volume for high-precision EBRT to treat coronary artery in-stent restenosis. The small dimension of the target volume warrants further exploration of this strategy.

References

1. Erikson U, Backlund L. Heart volume and its relation to age. Aspects of the technique. *Acta Radiol Diagn* 1981;22(5):541-543.
2. Farber LA, Bloch P, Yorke ED, Stevens CW, Herrmann H, Ruffer JE. A dosimetric comparison of conventional vs conformal external beam irradiation of a stented coronary artery utilizing a new fluoroscopic imaging detector system. *Cardiovasc Radiat Med* 1999;1(1):80-85.
3. Lax I, Blomgren H, Larson D, Näslund I. Extracranial stereotactic radiosurgery of localized targets. *J Radiosurg* 1998;1(2):135-148.
4. Leon MB, Teirstein PS, Moses JW, *et al.* Localized intracoronary gamma-radiation therapy to inhibit the recurrence of restenosis after stenting. *N Engl J Med* 2001;344(4):250-256.
5. Marijjanowski MM, Crocker IR, Styles T, *et al.* Fibrocellular tissue responses to endovascular and external beam irradiation in the porcine model of restenosis. *Int J Radiat Oncol Biol Phys* 1999;44(3):633-641.
6. Mazur W, Kaluza GL, Raizner AE. Radiation for the treatment of restenosis. In: Tripuraneni P, Jani S, Minar E, Leon M, editors. *Intravascular brachytherapy. From theory to practice*, 1st ed. London: ReMEDICA, 2001. pp. 167-187.
7. Potel MJ, Rubin JM, MacKay SA, Aisen AM, Al-Sadir J, Sayre RE. Methods for evaluating cardiac wall motion in three dimensions using bifurcation points of the coronary arterial tree. *Invest Radiol* 1983;18(1):47-57.
8. Schwartz RS, Koval TM, Edwards WD, *et al.* Effect of external beam irradiation on neointimal hyperplasia after experimental coronary artery injury. *J Am Coll Cardiol* 1992;19(5):1106-1113.
9. Slager CJ, Hooghoudt TE, Serruys PW, *et al.* Quantitative assessment of regional left ventricular motion using endocardial landmarks. *J Am Coll Cardiol* 1986;7(2):317-326.
10. Slager CJ, Wentzel JJ, Schuurbiens JC, *et al.* True 3-dimensional reconstruction of coronary arteries in patients by fusion of angiography and IVUS (ANGUS) and its quantitative validation. *Circulation* 2000;102(5):511-516.
11. Verheye S, Coussement PK, Salame MY, *et al.* High-dose external beam irradiation inhibits neointima formation in stented pig coronary arteries. *Int J Radiat Oncol Biol Phys* 2001;51(3):820-827.
12. Verin V, Popowski Y, de Bruyne B, *et al.* Endoluminal beta-radiation therapy for the prevention of coronary restenosis after balloon angioplasty. The Dose-Finding Study Group. *N Engl J Med* 2001;344(4):243-249.

13. Wang Y, Vidan E, Bergman GW. Cardiac motion of coronary arteries: variability in the rest period and implications for coronary MR angiography. *Radiology* 1999;213(3):751-758.
14. Wulf J, Hadinger U, Oppitz U, Olshausen B, Flentje M. Stereotactic radiotherapy of extracranial targets: CT-simulation and accuracy of treatment in the stereotactic body frame. *Radiother Oncol* 2000;57(2):225-236.

Chapter 3

A biplane angiographic study on cardiac motion of coronary artery stents: Options to minimize the target volume for high-precision external beam radiotherapy of coronary artery in-stent restenosis

Edward M. Leter
Johan C.H. Schuurbiens
Peter J.C.M. Nowak
Peter C. Levendag
Jolanda J. Wentzel
Peter M.T. Pattynama
Pim J. de Feijter
Patrick W. Serruys
Cornelis J. Slager

Int J Radiat Oncol Biol Phys 2004;58:278–283

Abstract

Purpose: High-precision external beam radiotherapy (EBRT) has been suggested as a potential alternative to endovascular brachytherapy for the treatment of coronary artery in-stent restenosis. The purpose of our study was to investigate and compare different options to define a smallest feasible target volume.

Methods and materials: The cardiac motion of 17 coronary artery stents in 17 patients was studied by use of biplane conventional angiography, recorded during breath-hold. Each stent was reconstructed in three dimensions by use of biplane sets of frames covering an entire cardiac cycle. The volume traversed by the stent during the entire or part of the cardiac cycle was determined. Four options to define the stent-traversed volume (STV) as a target for high-precision EBRT were investigated.

Results: The mean STV during the entire cardiac cycle was 3.5 cm³; the STV represented less than 1% of the heart volume in all patients. The STV during the diastolic and systolic phase resulted in a mean reduction of 26.6% and 29.1%, respectively, compared with the STV during the entire cardiac cycle. The smallest STV, measured during a 160-ms interval within the cardiac cycle, resulted in a mean maximal reduction of 75.9% compared with the STV during the entire cardiac cycle.

Conclusions: The STV during the entire cardiac cycle represents a small potential target volume for high-precision EBRT. A significant reduction of this target volume is possible in case of definition during a selected interval within the cardiac cycle.

Introduction

Endovascular brachytherapy is a potent therapeutic option for patients with coronary artery in-stent restenosis (1, 2). Nevertheless, external beam radiotherapy (EBRT) may offer radiobiological, physical, clinical, and logistic advantages over endovascular brachytherapy. The effectiveness of EBRT by delivery of a high single dose of 21 Gy to inhibit coronary artery in-stent restenosis has recently been reported in a porcine model. However, cardiac tissue side effects were also reported (3). The side effects in the latter study and in other studies (4, 5), which also investigated the use of EBRT targeted at the whole porcine heart, concurs with the well-established observation that the volume of heart irradiated is directly correlated with the risk of radiation-induced heart disease (6). Clinical implementation of EBRT as a potential alternative to intracoronary brachytherapy demands maximum effort to prevent such side effects, which can only be achieved by delivering EBRT to the smallest feasible target volume, such as a coronary artery stent. Hence exploration of high-precision EBRT has been suggested (3, 5, 7, 8). Because various strategies are available to reduce respiratory motion and novel strategies are being pursued (9), the main problem to overcome for such a treatment technique is to account for cardiac motion of coronary artery stents. Applying radiation to a volume covering successive stent locations enlarges the smallest possible target volume defined by the stent itself, but is likely to be required for practical application. Optimization of such a target volume requires data on cardiac motion of the stent in relation to time. For this purpose, the electrocardiogram (ECG) is useful as a means to indirectly infer the stent's continuous position throughout the cardiac cycle.

It has been recently shown that both biplane angiography (10) and multislice spiral computed tomography (MSCT) (11) synchronized to the ECG allow for definition of the volume through which coronary artery stents traverse during the entire cardiac cycle; the stent-traversed volume (STV) was reported to comprise less than 1% of the heart volume (HV). Reduction of this potential target volume for high-precision EBRT may be achieved by defining shorter intervals within the cardiac cycle. To date, this strategy has only been suggested (12, 13) and has not – to our knowledge – been investigated. The highest temporal resolution that can be provided by MSCT currently still is too low for a thorough investigation of the aforementioned strategy given the fast movement of coronary arteries; only X-ray angiography is suitable for such an investigation.

The purpose of this study was to use biplane X-ray angiograms to investigate and compare several options to define a smallest feasible target volume for high-precision EBRT of coronary artery in-stent restenosis.

Methods and materials

Patients

Seventeen coronary artery Wallstents (Schneider AG, Bülach, Switzerland) in 17 patients in sinus rhythm (13 men, 4 women) were studied by biplane angiography. The patients' ages were 57 ± 10 years (mean \pm 1 standard deviation [SD]), and their weight was 84 ± 11 kg. The stented vessels included the left circumflex ($n = 3$), the left anterior descending ($n = 6$), and the right coronary artery ($n = 8$). The stent diameter was 3.8 ± 0.6 mm, and the stent length was 31.9 ± 10.5 mm. The Erasmus MC Ethical Review Board approved the study, and informed consent was obtained from all participants.

Acquisition and processing of biplane angiography images

Biplane conventional X-ray angiography (BICOR, Siemens AG, Forchheim, Germany) of the stented coronary artery segment during breath-hold was performed at 25 frames/s. From the film recordings, biplane sets of contrast-free frames clearly showing the stent and covering an entire cardiac cycle plus seven additional frames before and after the R-peak in the ECG were selected and stored on a personal computer. The borders of the stent were contoured manually in the selected sets of frames (Figure 1). For contour determination custom-made software was used incorporating standard zooming and contrast optimization features to aid recognition of image details.

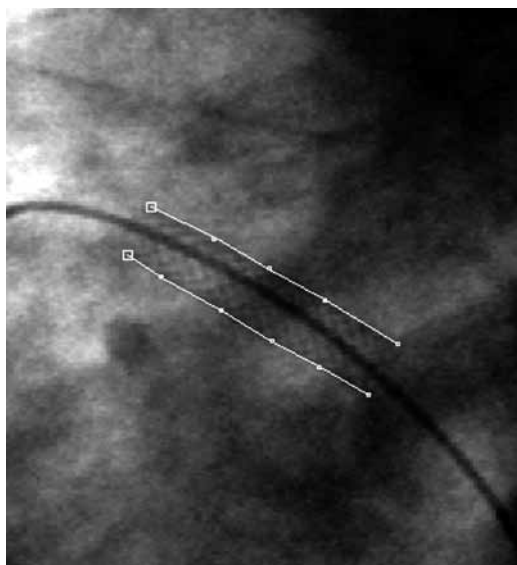


Figure 1. Lateral angiographic view of a contoured left circumflex coronary artery stent.

Three-dimensional reconstruction of coronary artery stents and stent traversed volumes

The method to three-dimensionally (3D) reconstruct coronary artery stents uses the algorithm previously described to 3D reconstruct the centerline of an intravascular ultrasound catheter (14). The centerline of the stent and its diameter in each biplane view was derived from the stent contours. By use of these centerlines, the 3D centerline can be reconstructed. The stent length was determined by measurement of the length of the reconstructed centerline. By combining the angiographically determined stent diameter with the 3D centerline, a cylindrical 3D stent body was reconstructed. Calculation of the stent volume was performed by determination of all voxels in 3D space (0.5 mm cubic resolution) encompassed by the cylindrical stent body.

For the moving stent, positions in between two successive locations were interpolated at a spatial resolution less than 0.5 mm. Combining all voxels traversed by the moving stent with those encompassed by the stent itself at its first and final position of a certain trajectory defined the STV (Figure 2).

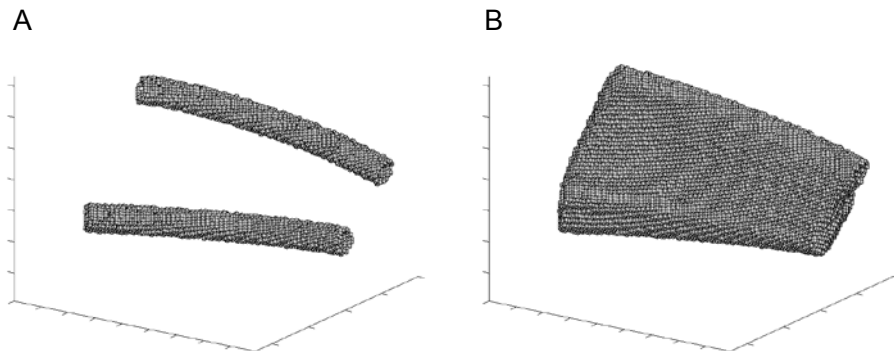


Figure 2. Diagram shows the definition of the stent-traversed volume during the entire cardiac cycle for a right coronary artery stent. (a) Voxels encompassed by the stent itself at its first and final position. (b) All voxels traversed by the moving stent including those encompassed by the stent itself at its first and final position of a certain trajectory.

Data analysis

Three-dimensional displacement and velocity of the proximal and distal stent ends throughout the cardiac cycle was measured relative to the first defined end diastolic location (R-peak). Four options to define the target volume for high-precision EBRT were investigated:

1. The STV during the entire cardiac cycle.
2. The STV during the diastolic phase of the cardiac cycle. The diastolic phase was defined by use of velocity plots (Figure 3), and its duration was measured.

3. The STV during the systolic phase of the cardiac cycle. The systolic phase was defined by use of velocity plots (Figure 3), and its duration was measured.
4. The smallest STV during 160-480-ms intervals when moving by 40-ms steps through the cardiac cycle (Figure 4). For each patient, the time between the first defined R-peak and the time point at which the smallest STV was observed was expressed relative to the duration of the RR interval.

For the latter three options – that is, high-precision EBRT during intervals shorter than the cardiac cycle – the elongation factor of the irradiation time relative to delivering the same dose during the entire cardiac cycle was calculated.

An estimate of the HV was calculated by the equations as have been reported by Erikson *et al.* (15).

Statistical analysis

All values are expressed as mean \pm SD. The paired *t* test was used to compare the STVs between the different options to define the target volume. A value of $p < 0.05$ was considered significant.

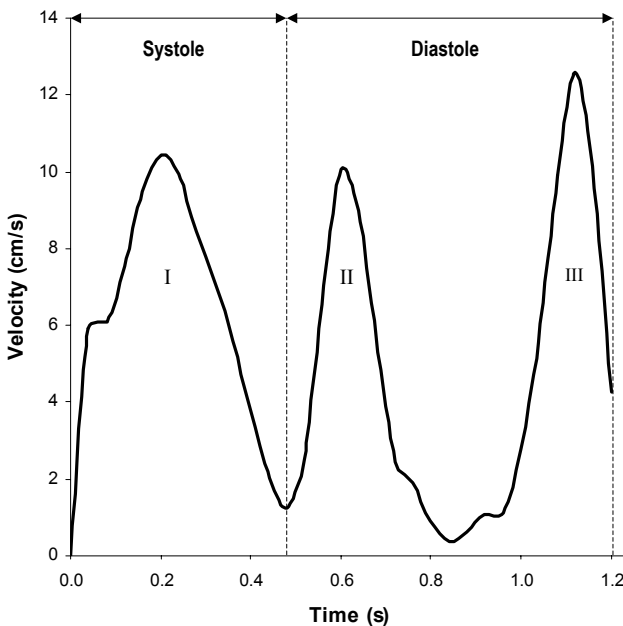


Figure 3. The velocity of a right coronary artery distal stent end throughout the cardiac cycle. The typical velocity plot is triphasic with peaks during the systole (I), early diastole (II), and atrial contraction (III) (20). These peaks enable differentiation between the systolic and diastolic phase of the cardiac cycle, as is also depicted in the diagram.

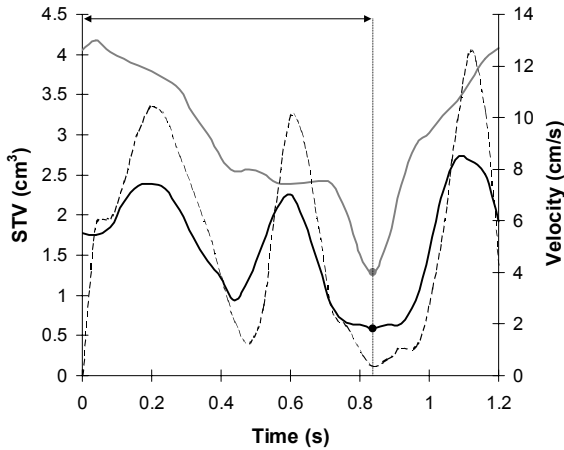


Figure 4. The stent-traversed volume (STV) for a right coronary artery (RCA) stent throughout the cardiac cycle for a 160- (black line) and 400-ms (gray line) interval. The point that corresponds to the smallest STV for the respective intervals is depicted by a dot. Also shown is the velocity of the proximal stent end (dotted line) throughout the cardiac cycle. The pattern of the graph line for the 160-ms interval and velocity is quite similar, in contrast to the graph line for the 400-ms interval and velocity. The time between the first defined R-peak and the time point within the cardiac cycle at which the smallest STV was observed was measured (arrow).

Results

The STV during the entire cardiac cycle was $3.5 \pm 2.6 \text{ cm}^3$. For all patients, the STV represented less than 1% of the HV. The estimated HV was $1264 \pm 212 \text{ cm}^3$. The duration of the entire cardiac cycle was $0.96 \pm 0.18 \text{ s}$.

The STV during the diastolic phase of the cardiac cycle was $2.5 \pm 1.9 \text{ cm}^3$, which corresponded to a reduction of $26.6 \pm 11.7\%$ in comparison to that during the entire cardiac cycle. For all patients, the STV during the diastolic phase represented less than 0.5% of the HV. The duration of the diastolic phase was $0.59 \pm 0.14 \text{ s}$. In comparison to high-precision EBRT of the STV during the entire cardiac cycle, targeting the STV during the diastolic phase would increase the irradiation time by a factor of 1.7 ± 0.2 .

The STV during the systolic phase of the cardiac cycle was $2.4 \pm 1.6 \text{ cm}^3$, which corresponded to a reduction of $29.1 \pm 10.3\%$ in comparison to that during the entire cardiac cycle. For all patients, the STV during the systolic phase represented less than 0.5% of the HV. The duration of the systolic phase was $0.39 \pm 0.08 \text{ s}$. In comparison to high-precision EBRT of the STV during the entire cardiac cycle, targeting the STV during the systolic phase would increase the irradiation time by a factor of 2.5 ± 0.4 .

The smallest STV during 480-ms, 400-ms, 320-ms, 240-ms, and 160-ms intervals within the cardiac cycle was $1.5 \pm 1.1 \text{ cm}^3$, $1.5 \pm 1.0 \text{ cm}^3$, $1.2 \pm 0.9 \text{ cm}^3$, $0.9 \pm 0.6 \text{ cm}^3$, and $0.7 \pm 0.4 \text{ cm}^3$, respectively, which corresponded to a reduction of $46.5 \pm 16.3\%$, $54.1 \pm 15.9\%$, $61.8 \pm 14.4\%$, $68.6 \pm 13.0\%$, and $75.9 \pm 10.0\%$, respectively, in comparison to the STV during the entire cardiac cycle. For all patients, the STV during all intervals represented less than 0.3% of the HV, reaching a minimum of $0.06 \pm 0.03\%$ for the shortest interval. The time point at which the smallest STV was observed was at $54 \pm 18\%$, $51 \pm 17\%$, $52 \pm 16\%$, $54 \pm 16\%$, and $54 \pm 17\%$ of the RR interval for the 160–480-ms intervals, respectively. In comparison to high-precision EBRT of the STV during the entire cardiac cycle, targeting the STV during a 160–480-ms interval within the cardiac cycle would increase the irradiation time by a factor ranging between 6.2 ± 1.0 and 2.1 ± 0.3 . Intervals larger than 480 ms resulted in a steep rise of the corresponding STV. Therefore larger intervals were not investigated. The smallest possible STV, that is, the stent volume itself, was $0.4 \pm 0.2 \text{ cm}^3$.

The STV steadily decreased significantly with each option to define the target volume (i.e., from the STV measured during the entire cardiac cycle to the smallest STV measured during a 160-ms interval within the cardiac cycle) with exception of the difference between the STV during the diastolic and systolic phase.

Discussion

Because of its superior image quality and temporal resolution, biplane angiography was chosen to investigate four different options to define the STV during all or part of the cardiac cycle. It is shown that biplane angiography allowed definition of significantly smaller potential target volumes when compared with the STV during the entire cardiac cycle. Measurement of the STV during the diastolic and systolic phase of the cardiac cycle resulted in a mean reduction of 26.6% and 29.1%, respectively, in comparison to the STV during the entire cardiac cycle. The smallest STV during the shortest investigated interval of 160 ms within the cardiac cycle resulted in a mean maximal reduction of the STV by 75.9% in comparison to the STV during the entire cardiac cycle.

Because most, if not all, coronary artery stents will not be visible on conventional portal films, an alternative strategy is needed for treatment setup verification and correction. Systems combining biplane X-ray imaging with an image-guided linear accelerator have recently been introduced in radiotherapy and may use the findings of the current study. The real-time tumor-tracking radiotherapy system, for instance, consists of two pairs of diagnostic X-ray systems, an image processor

unit, a gating control unit, and an image display unit. The system recognizes the position of a 2.0-mm gold marker, which is inserted in or near a body tumor 30 times per second. The linear accelerator is gated to irradiate the tumor only when the marker is within a given tolerance from its planned coordinates relative to the isocenter (16). An exactly similar strategy would not be applicable for ECG-triggered high-precision EBRT of coronary artery stents because the radiopacity of current stents will not allow real-time 3D reconstruction. It neither is likely that markers could be added to stents considering space and biocompatibility restrictions. An adaptation of real-time tumor-tracking radiotherapy on the other hand seems feasible. To use the optimum cardiac window as determined in this study, respiratory motion would need to be reproducibly accounted for during high-precision EBRT treatment planning and treatment. Either respiratory triggering or a breath-hold technique can be used for this purpose. Cardiac triggering combined with a breath-hold technique would be preferable from a technical point of view. However, the latter is notoriously irreproducible without a spirometry forced breath-hold (9). Active breathing control may therefore be useful because it allows temporary and reproducible immobilization of internal thoracic structures by implementing breath-hold at a predefined phase within the breathing cycle (17). During such breath-holds, ECG-triggered pulses of irradiation can be applied during a specific interval within successive cardiac cycles. The 3D stent locations during the interval selected during treatment planning would need to be determined before irradiation from biplane images while the patient maintains the predefined breath-hold. The STV can then be defined using these 3D stent locations, which at most will take about 1 min, and could subsequently be targeted by ECG-triggered pulses during the selected interval within successive cardiac cycles. Whether additional reduction of the STV may be achieved for any interval by taking into account the specific shape of the STV and direction of cardiac motion in selecting beam directions needs further study. In any case, it is anticipated that the aforementioned irradiation strategy will significantly reduce the 3D planning target volume margin that includes all treatment uncertainties. Coronary arteries have been reported to return to the same position from heartbeat to heartbeat with great precision during breath-hold (18). However, it remains to be investigated whether the time point at which the smallest STV was measured for intervals within the cardiac cycle can be reproducibly inferred from the ECG.

Because biplane X-ray imaging data are not directly compatible with EBRT treatment planning systems, computed tomography data would be needed. Moreover, accurate treatment planning calculations would benefit from computed tomography images that clearly show cardiac vessel anatomy including stents besides other thoracic structures. ECG-gated MSCT is suitable for this purpose

because it allows reliable noninvasive coronary artery imaging (19). MSCT scans for treatment planning would be acquired during a selected interval within the cardiac cycle while the patient maintains the predefined breath-hold. Because the highest temporal resolution MSCT currently allowed is about 200 ms, some enlargement of the minimal STV determined for an interval of, for example, 160 ms, is anticipated. Nevertheless, it seems a fair anticipation that MSCT will allow reasonably accurate treatment planning. Furthermore, the number of MSCT scanners installed around the world is growing exponentially and the gap between the temporal resolution of MSCT and biplane X-ray imaging as used in this study will be closed even further in the near future. Alternatively, the angiographically defined STV could be superimposed on planning computed tomography images that would only need to allow identification of the external patient contour, lung and heart tissues.

Although ECG-triggered irradiation of target volumes defined during intervals of, for example, 160 ms, may be essential in an attempt to minimize potential radiation-induced heart disease and is within the specifications of state-of-the-art linear accelerators with ultrafast beam-on times, such a strategy will technically be quite challenging. To what extent targeting the STV during part instead of during the entire cardiac cycle would result in a proportionate reduction of the volume of heart exposed to the prescribed dose needs to be studied. ECG-triggered irradiation during small intervals within the cardiac cycle will also demand great logistic efforts. When high-precision ECG-triggered EBRT would be applied during 160-ms intervals, irradiation time will increase by a mean maximal factor of 6.2 in comparison to treatment during the entire cardiac cycle. Delivery of 10 Gy, for instance, with a dose rate of 600 MU/min takes 3–5 min for one static beam. Considering irradiation time only, ECG-triggered EBRT with one static beam during 160-ms intervals would therefore increase treatment duration to 18–30 min at least. This would impose a heavy burden on the logistics of a radiotherapy unit; especially when additional logistically imposing factors are considered such as dose fractionation, treatment with multiple beams to minimize the volume of heart receiving high dose as much as possible and repeated preparations of cardiac triggering combined with active breathing control.

In conclusion, biplane X-ray imaging allows definition of the STV during the entire cardiac cycle, which represents a small potential target volume for high-precision EBRT. A significant reduction of this target volume is possible by selecting an interval within the cardiac cycle. ECG-triggered EBRT of such small target volumes for treatment of coronary artery in-stent restenosis seems feasible but will require complex technical and logistic efforts.

References

1. Verin V, Popowski Y, de Bruyne B, *et al.* Endoluminal beta-radiation therapy for the prevention of coronary restenosis after balloon angioplasty. The Dose-Finding Study Group. *N Engl J Med* 2001;344:243-249.
2. Leon MB, Teirstein PS, Moses JW, *et al.* Localized intracoronary gamma-radiation therapy to inhibit the recurrence of restenosis after stenting. *N Engl J Med* 2001;344:250-256.
3. Verheye S, Coussement PK, Salame MY, *et al.* High-dose external beam irradiation inhibits neointima formation in stented pig coronary arteries. *Int J Radiat Oncol Biol Phys* 2001;51:820-827.
4. Schwartz RS, Koval TM, Edwards WD, *et al.* Effect of external beam irradiation on neointimal hyperplasia after experimental coronary artery injury. *J Am Coll Cardiol* 1992;19:1106-1113.
5. Marijianowski MM, Crocker IR, Styles T, *et al.* Fibrocellular tissue responses to endovascular and external beam irradiation in the porcine model of restenosis. *Int J Radiat Oncol Biol Phys* 1999;44:633-641.
6. Stewart JR, Fajardo LF, Gillette SM, *et al.* Radiation injury to the heart. *Int J Radiat Oncol Biol Phys* 1995;31:1205-1211.
7. Williams JP, Eagleton MJ, Hernady E, *et al.* Effectiveness of fractionated external beam radiation in the inhibition of vascular restenosis. *Cardiovasc Radiat Med* 1999;1:257-264.
8. Mazur W, Kaluza GL, Raizner AE. Radiation for the treatment of restenosis. In: Tripuraneni P, Jani S, Minar E, Leon M, editors. *Intravascular brachytherapy. From theory to practice.* London: ReMEDICA Publishing Limited; 2001. p. 167-187.
9. Ozhasoglu C, Murphy MJ. Issues in respiratory motion compensation during external-beam radiotherapy. *Int J Radiat Oncol Biol Phys* 2002;52:1389-1399.
10. Leter EM, Schuurbijs JCH, Nowak PJCM, *et al.* Coronary stent traversed volume during the cardiac cycle defined as a target for high-precision radiotherapy by using biplane angiograms. *Radiother Oncol* 2002;63:103-106.
11. Leter EM, Nowak PJ, Nieman K, *et al.* Definition of a moving gross target volume for stereotactic radiation therapy of stented coronary arteries. *Int J Radiat Oncol Biol Phys* 2002;52:560-565.
12. Farber LA, Bloch P, Yorke ED, *et al.* A dosimetric comparison of conventional vs conformal external beam irradiation of a stented coronary artery utilizing

- a new fluoroscopic imaging detector system. *Cardiovasc Radiat Med* 1999;1:80-85.
13. Tallman MP, Williams JP, Hernady E, *et al.* Tolerance of normal rabbit femoral arteries to single high dose external beam irradiation. *Cardiovasc Radiat Med* 1999;1:131-137.
 14. Slager CJ, Wentzel JJ, Schuurbiens JC, *et al.* True 3-dimensional reconstruction of coronary arteries in patients by fusion of angiography and IVUS (ANGUS) and its quantitative validation. *Circulation* 2000;102:511-516.
 15. Erikson U, Backlund L. Heart volume and its relation to age. Aspects of the technique. *Acta Radiol Diagn* 1981;22:541-543.
 16. Shirato H, Shimizu S, Shimizu T, *et al.* Real-time tumour-tracking radiotherapy. *Lancet* 1999;353:1331-1332.
 17. Wong JW, Sharpe MB, Jaffray DA, *et al.* The use of active breathing control (ABC) to reduce margin for breathing motion. *Int J Radiat Oncol Biol Phys* 1999;44:911-919.
 18. Wang Y, Vidan E, Bergman GW. Cardiac motion of coronary arteries: variability in the rest period and implications for coronary MR angiography. *Radiology* 1999;213:751-758.
 19. Nieman K, Cademartiri F, Lemos PA, *et al.* Reliable noninvasive coronary angiography with fast submillimeter multislice spiral computed tomography. *Circulation* 2002;106:2051-2054.
 20. Potel MJ, Rubin JM, MacKay SA, *et al.* Methods for evaluating cardiac wall motion in three dimensions using bifurcation points of the coronary arterial tree. *Invest Radiol* 1983;18:47-57.

Chapter

4

Definition of a moving gross target volume for stereotactic radiation therapy of stented coronary arteries

Edward M. Leter
Peter J.C.M. Nowak
Koen Nieman
Pim J. de Feyter
Stéphane G. Carlier
Aristoteles Munne
Patrick W. Serruys
Peter C. Levendag

Int J Radiat Oncol Biol Phys 2002;52:560–565

Abstract

Purpose: To measure the effect of cardiac motion on coronary artery stent position during the cardiac cycle as a first step toward exploring the feasibility of stereotactic external beam radiation therapy targeted at restenotic stented coronary arteries.

Methods and materials: The three-dimensional (3D) position of eight coronary artery stents in 8 patients immobilized in a stereotactic body frame was studied noninvasively by single-breathhold ECG-gated multislice spiral computed tomography (MSCT) during 10 retrospectively selected phases, equally distributed throughout the R-R interval of consecutive cardiac cycles. The volume encompassing all measured 3D positions of the stent was measured.

Results: Stent volumes measured by MSCT closely agreed with measurements by quantitative coronary angiography ($r > 0.99$). The mean of the maximum 3D stent center of mass displacement between any two phases during the cardiac cycle for all eight coronary arteries was 7.5 mm (range 3.3–20.5 mm) in the lateral direction, 8.6 mm (range 2.7–21.6 mm) in the ventrodorsal direction, and 8.2 mm (range 2.5–19.7 mm) in the craniocaudal direction. As was anticipated, the volume encompassing all measured 3D positions of the stent represented only a fraction of the whole heart volume in all patients, i.e., less than 0.6 %.

Conclusions: ECG-gated MSCT allowed the measurement of the volume encompassing multiphase 3D positions of coronary artery stents during the cardiac cycle. This volume, a measure of the cardiac motion effect on coronary artery stent position during the cardiac cycle, represents a moving gross target for stereotactic external beam radiation therapy.

Introduction

In-stent restenosis after successful intracoronary stent implantation is a serious medical condition. Despite the use of repeated interventional procedures, > 50% of these patients have recurrent in-stent restenosis (1). Several randomized clinical trials have demonstrated that intracoronary γ - and β -radiation, as an adjunct modality to intervention, are potent new therapies for in-stent restenosis (2-4). For example, Leon *et al.* (2) have demonstrated that the need for repeated revascularization of the target lesion was reduced by 42%. However, new phenomena arise: late stent thrombosis caused by radiation-induced delay in endothelialization over the stent struts or by the effects of radiation on endothelial-cell function may emerge (2). In addition endovascular brachytherapy suffers from several biologic, physical, and logistic disadvantages that – in theory – could be bypassed by the use of external beam radiation therapy (EBRT). Among the advantages EBRT offers over endovascular brachytherapy are its noninvasive nature, improved dose homogeneity and accuracy over a range of tissue depths, flexibility to optimize the time of treatment in relation to target cell proliferation after percutaneous transluminal coronary angioplasty, dose fractionation, and use of radiosensitizers. Moreover, EBRT has demonstrated reduced postangioplasty restenosis in peripheral vessels (5, 6). To date, no studies have reported beneficial effects of EBRT in coronary arteries. Marijianowski *et al.* (7), for instance, reported that EBRT in pig coronary arteries could exacerbate arterial healing, evidenced by the presence of interstitial and perivascular fibrosis in the myocardium. The authors argued that this result might be explained by their irradiation technique; virtually the whole heart received the prescribed dose of 14 Gy, while it is well established that the volume of heart irradiated is directly correlated with the risk of radiation-induced cardiotoxicity (8). Hence stereotactic EBRT, e.g., targeted at the volume encompassing all three-dimensional (3D) positions of a coronary artery stent during the cardiac cycle, has been suggested as a potential future direction to pursue (9, 10). Such a strategy will present several challenging problems such as measurement of the cardiac and respiratory motion effect on coronary artery stent position, and precise and reproducible setup accuracy.

The purpose of this study was to determine whether electrocardiographically (ECG)-gated multislice spiral computed tomography (MSCT) of stented coronary arteries in patients immobilized in a stereotactic body frame (SBF) allowed us to measure the effect of cardiac motion on coronary artery stent position during the cardiac cycle. This is a first step toward exploring the feasibility of stereotactic EBRT targeted at restenotic stented coronary arteries.

Methods and materials

Patients

The University Hospital Ethical Review Board approved this study. All participants gave informed consent. Between February 1 and April 11, 2000, eight consecutive patients (two women and six men, age range 48–75 years, mean age 59 years) referred by the cardiologist for evaluation of coronary artery stenoses by contrast-enhanced MSCT, were entered in this study. A single stent was studied in each patient, one in the left circumflex (LCx), five in the left anterior descending (LAD) and two in the right coronary artery (RCA). The following eight, stainless-steel stents were used: three NIROYAL (Medinol, Maple Grove, MN), two ACS Multi-link Duet (Guidant, Santa Clara, CA), one Genius (EuroCor, Bonn, Germany), one BX Velocity (Cordis, Warren, NJ), and one Terumo (Terumo, Tokyo, Japan). The mean nominal stent length was 23 mm (range 16–38 mm). The median interval between stent implantation and the MSCT scan was 19.5 days (range 3–89 days). All patients were in sinus rhythm with mean heart rates between 57 and 93 beats per minute.

Stereotactic body frame

The SBF (Elekta, Crawley, West Sussex, UK) has been described previously in detail (11). Briefly, on the table of the MSCT scanner, patients were positioned in the SBF on a vacuum pillow filled with plastic pellets. The pillow was shaped to the patient's body by allowing air to enter. The air was evacuated out of the pillow by a manual pump to obtain a rigid body mold. The 3D coordinate system, manufactured to be visualized on CT images and mounted inside the SBF side walls, was subsequently aligned to the MSCT gantry laser. By using the level control and a spirit level, the SBF was finally also accurately aligned to the horizontal plane.

Multislice computed tomography: Data acquisition and image reconstruction

The MSCT scanner (SOMATOM Volume Zoom, Siemens AG, Forchheim, Germany) with a 500-ms rotation time and simultaneous acquisition of four slices, has been described previously (12–14). Briefly, 20 s after the i.v. injection of 150 mL of contrast agent (iomeprol, Iomeron 350 mg iodine/mL, Bracco, Milan, Italy), the scan was initiated with simultaneous registration of the patient's ECG signal. Contrast-enhancement was used to enable identification of all major epicardial vessels, which is essential for future dosimetric studies. Within a single end-inspiratory breathhold (range 27–41 s, mean 35 s), the entire heart volume was scanned with a 4 x 1-mm collimation protocol (effective slice thickness 1.25 mm). The pitch (table feed per rotation divided by the single collimated slice thickness)

was set at 1.5 for heart rates below 80 beats per min (7 patients) and 2.0 for faster heart rates (1 patient). The raw CT data were transferred to an off-line PC workstation for ECG-gated image reconstruction by dedicated work-in-progress software (Siemens Cardio Package, Siemens AG) implemented in MATLAB V5.3 (MathWorks Inc, Natick, MA). Isocardiophasic, overlapping (increment 0.8 mm), axial slices (field of view 80 mm; matrix 512 x 512) were reconstructed during 10 retrospectively selected, 250-ms-long intervals (partial scan-reconstruction techniques, which apply a 90–180° reconstruction algorithm, improve the temporal resolution to 250 ms) equally distributed throughout the R-R interval of the consecutive cardiac cycles. The phases were determined relative to the previous R peak for each cardiac cycle separately, with starting points given as a percentage of the R-R interval (Figure 1).

Quantitative coronary angiography (QCA)

By use of the interventional angiograms, the mean stent diameter was determined in a single end-diastolic image with an edge detection quantitative angiography system (CAAS II, Pie Medical, Maastricht, The Netherlands) (15). The empty catheter was used for calibration. The stent volume, computed by $\pi r^2 l$ (r = mean QCA stent radius, l = nominal stent length provided by the manufacturer), is referred to as the QCA stent volume and represents an estimate of the true stent volume. The primary reason to use the nominal stent length was to avoid the effects of foreshortening (measurement of a shortened stent when the angiographic plane of view is not exactly parallel to the length of the stent) associated with QCA.

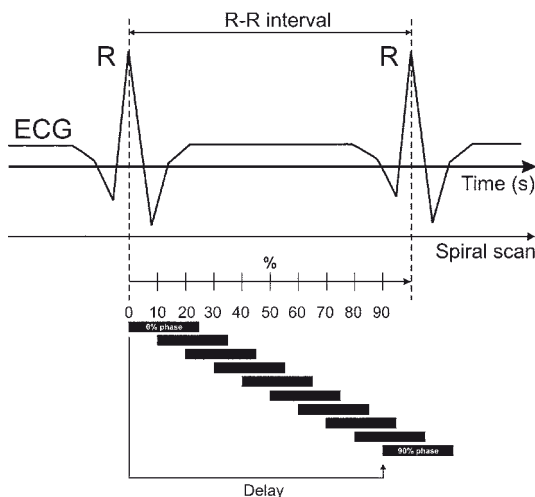


Figure 1. Strategy to determine 3D stent center of mass displacements; image datasets were reconstructed during 10 cardiac phases.

Data analysis

The reconstructed DICOM (digital imaging and communications in medicine) images were transferred to a XKnife 4.0 3D radiosurgery planning workstation (Radionics, Burlington, MA). Cardiac motion and local metal artifacts around the stent struts were observed; the stent wall was manually contoured across its centerline at a level of around 400 Hounsfield units in all 10 MSCT datasets of each patient (Figure 2a). By use of the contours, the radiosurgery planning software constructed stent volumes.

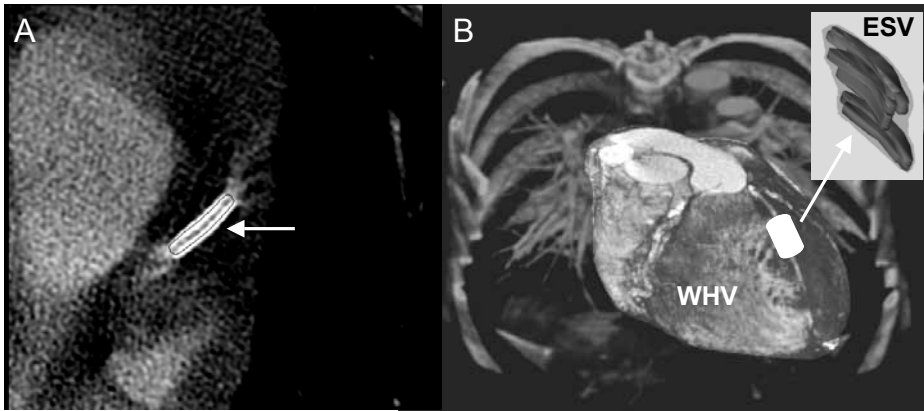


Figure 2. (a) Multislice CT image of a left anterior descending coronary artery stent contoured in black (arrow). (b) Whole heart volume (WHV) and volume encompassing all measured 3D positions (ESV) of a left anterior descending coronary artery stent during the cardiac cycle.

The dataset that visually yielded optimal image quality was used to measure the reference stent volume with use of custom-made software developed by one of the authors. This volume was considered to represent the MSCT stent volume, and was consecutively matched by 3D translation and rotation with the other nine volumes to measure the stent center of mass displacements throughout the cardiac cycle. The matches were visually verified to preclude displacements attributable to differences in stent volume. For each patient, the stent volumes of all datasets were copied to one image. The volume around all 10 stent positions was encompassed as a measure of the cardiac motion effect during contraction (systole) and relaxation (diastole).

This volume was compared with the whole heart volume (including the pulmonary trunk, ascending aorta, and superior vena cava beginning on the cross-section in which the left auricle emerged, and then following the external contour of the heart caudally), which was contoured slice-by-slice in an additionally reconstructed dataset (Figure 2b).

Statistical analysis

Regression analysis was used to determine the correlation between QCA and MSCT stent volume measurements. The agreement between measurement by QCA and MSCT was quantified using the differences between observations made using the two methods on the same subjects (16).

Results

The imaging procedure with the SBF was performed successfully and without complications in all patients. ECG-gated MSCT provided adequate image quality for multiphase visualization of coronary artery stents.

A close linear correlation ($r > 0.99$) between QCA and MSCT measurements of stent volumes was found (Figure 3a). MSCT consistently overestimated the QCA stent volumes (Figure 3b); the between-method difference was $46.6 \pm 1.4 \text{ mm}^3$ (SD). In an attempt to explain the consistent overestimation, the stent volumes were also measured in images reconstructed by use of a smoother kernel with a higher signal-to-noise ratio. Again, a close linear correlation ($r > 0.99$) was found (Figure 3a). MSCT consistently slightly underestimated the QCA stent volumes (Figure 3b); the between-method difference was $-5.4 \pm 2.7 \text{ mm}^3$ (SD).

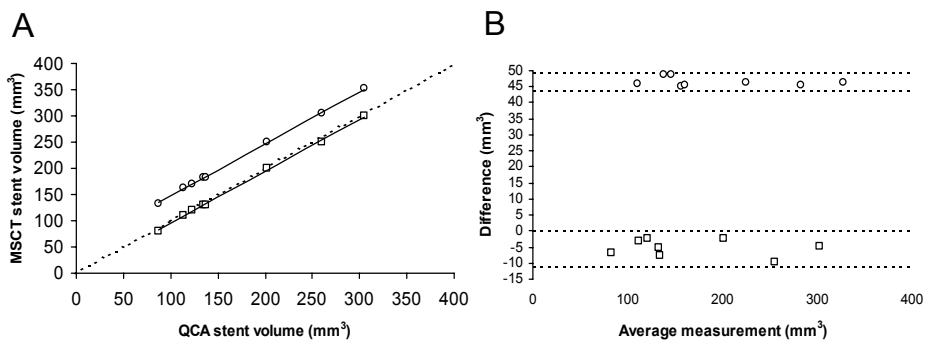


Figure 3. Correlation between stent volumes measured by quantitative coronary angiography and multislice CT. (a)

Regression analysis to determine linear correlation. The dotted line indicates equality. (b) Between-method difference plotted against the average of corresponding measurements (16). The dotted horizontal lines indicate the mean between-method difference \pm 2 standard deviations. \oplus = stent volumes measured in images reconstructed by the original kernel; \square = stent volumes measured in images reconstructed by the smoother kernel.

The mean of the maximum 3D stent center of mass displacement between any two phases during the cardiac cycle for all eight coronary arteries was 7.5 mm (range 3.3–20.5 mm) in the lateral direction, 8.6 mm (range 2.7–21.6 mm) in

the ventrodorsal direction, and 8.2 mm (range 2.5–19.7 mm) in the craniocaudal direction (Figure 4). The mean of the volume encompassing all measured 3D stent positions was 1.4 cm³ (range 0.4–3.8 cm³). The mean whole heart volume was 740 cm³ (range 683–828 cm³). As was anticipated, the volume encompassing all measured 3D positions of the stent represented only a fraction of the whole heart volume in all patients, that is, less than 0.6 %.

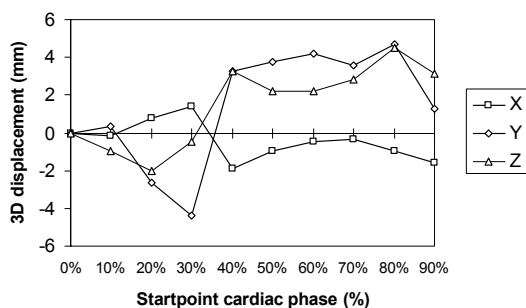


Figure 4. Representative 3D displacement pattern throughout the cardiac cycle of a left anterior descending coronary artery stent center of mass. The position of the stent center of mass was measured during 10 cardiac phases equally distributed throughout the R-R interval. All plots are normalized to 0 %, i.e., normalized to the R peak that reflects the onset of ventricular activation. The x-dimension designates lateral displacement, the y-dimension ventrodorsal displacement, and the z-dimension craniocaudal displacement. Positive x, y and z values correspond to left, dorsal, and cranial displacements, respectively. The amplitude of the displacement in each dimension reflects the maximum displacement between any two phases during the cardiac cycle (19).

Discussion

Because of the potential advantages of EBRT over endovascular brachytherapy, stereotactic EBRT, e.g., targeted at the volume encompassing all 3D positions of a coronary artery stent during the cardiac cycle, has been suggested as a potential future direction to pursue in cardiovascular radiation medicine for in-stent restenosis (9, 10). The present study demonstrates that ECG-gated MSCT allowed the measurement of the volume encompassing multiphase 3D positions of a coronary artery stent during the cardiac cycle, as a measure of the cardiac motion effect. As was anticipated, this volume represented only a fraction of the whole heart volume in all patients. The definition of this moving gross target volume (GTV) represents a first step toward exploring the feasibility of stereotactic EBRT targeted at restenotic stented coronary arteries. To our knowledge, measurement of such a moving GTV, by using imaging data indexed in time with the ECG, has not been reported previously.

However, further refinement is needed, e.g., of the stent volume measurement by MSCT, and other challenging problems need to be overcome, such as accounting for the effect of respiratory motion on coronary artery stent position during the cardiac cycle and for stereotactic setup accuracy. The SBF used for this study may be useful to partly overcome these challenging problems as it provides precise and reproducible 3D setup accuracy of less than 5 mm (SD) (11, 17).

A limitation of this study relates to the measured stent positions that in fact represent an average position during each cardiac phase, because the current 250-ms temporal resolution of MSCT allows considerable coronary artery motion. On the other hand, MSCT allows retrospectively ECG-gated multiphase spiral data acquisition, offers high spatial resolution, low image noise, and high tissue contrast compared to other noninvasive cardiac imaging techniques such as electron-beam computed tomography and magnetic resonance imaging (12–14). Furthermore, MSCT data are compatible with EBRT planning systems. Because of the small number of patients, we could not provide stent center of mass displacement and encompassing volume data for each of the major epicardial coronary arteries separately, i.e., LCx, LAD and RCA. As opposed to the LAD, the RCA runs through the atrioventricular sulcus in the basal plane of the heart. Because cardiac motion increases from apex to base (18), higher volumes encompassing all 3D positions of a coronary artery stent during the cardiac cycle in the case of RCA compared to LAD stents are to be expected. In addition, the anatomic course of the RCA has an almost perpendicular orientation to the main direction of cardiac motion, i.e., from basal plane to apex (18), whereas the LAD has a more parallel orientation to the main direction of cardiac motion. This difference in orientation of the RCA and LAD in relation to the main direction of cardiac motion will also add to a difference in volumes encompassing all 3D positions of RCA and LAD stents during the cardiac cycle. Although the number of patients studied was small, the observed range, direction, and variation of 3D coronary artery stent displacements were in agreement with previously reported data (19). The effect of respiratory motion on coronary artery position during the cardiac cycle was not yet accounted for in this study, but will be addressed in future studies. This effect may be accounted for by use of active breathing control, which allows temporary and reproducible immobilization of internal thoracic structures by implementing a breathhold at a preselected phase in the breathing cycle (20), or by respiratory-gating techniques.

In conclusion, the results represent a first step toward exploring the feasibility of stereotactic EBRT of restenotic stented coronary arteries, i.e., the definition of a moving GTV. We believe this strategy deserves further investigative exploration.

References

1. Reimers B, Moussa I, Akiyama T, *et al.* Long-term clinical follow-up after successful repeat percutaneous intervention for stent restenosis. *J Am Coll Cardiol* 1997;30:186-192.
2. Leon MB, Teirstein PS, Moses JW, *et al.* Localized intracoronary gamma-radiation therapy to inhibit the recurrence of restenosis after stenting. *N Engl J Med* 2001;344:250-256.
3. Waksman R, White RL, Chan RC, *et al.* Intracoronary gamma-radiation therapy after angioplasty inhibits recurrence in patients with in-stent restenosis. *Circulation* 2000;101:2165-2171.
4. Verin V, Popowski Y, de Bruyne B, *et al.* Endoluminal beta-radiation therapy for the prevention of coronary restenosis after balloon angioplasty. The Dose-Finding Study Group. *N Engl J Med* 2001;344:243-249.
5. Oh YT, Kim HS, Chun M, *et al.* The effect of external electron beam on neointima in rat carotid artery injury model. *Int J Radiat Oncol Biol Phys* 1999;44:643-648.
6. Mayberg MR, London S, Rasey J, *et al.* Inhibition of rat smooth muscle proliferation by radiation after arterial injury: temporal characteristics in vivo and in vitro. *Radiat Res* 2000;153:153-163.
7. Marijianowski MM, Crocker IR, Styles T, *et al.* Fibrocellular tissue responses to endovascular and external beam irradiation in the porcine model of restenosis. *Int J Radiat Oncol Biol Phys* 1999;44:633-641.
8. Stewart JR, Fajardo LF, Gillette SM, *et al.* Radiation injury to the heart. *Int J Radiat Oncol Biol Phys* 1995;31:1205-1211.
9. Mazur W, Kaluza GL, Raizner AE. Radiation for the treatment of restenosis. In: Tripuraneni P, Jani S, Minar E, Leon M, editors. *Intravascular brachytherapy: From theory to practice*. 1st ed. London: ReMEDICA Publishing; 2001. p. 167-187.
10. Farber LA, Bloch P, Yorke ED, *et al.* A dosimetric comparison of conventional vs conformal external beam irradiation of a stented coronary artery utilizing a new fluoroscopic imaging detector system. *Cardiovasc Radiat Med* 1999;1:80-85.
11. Lax I, Blomgren H, Larson D, *et al.* Extracranial stereotactic radiosurgery of localized targets. *J Radiosurg* 1998;1:135-148.
12. Achenbach S, Ulzheimer S, Baum U, *et al.* Noninvasive coronary angiography by retrospectively ECG-gated multislice spiral CT. *Circulation* 2000;102:2823-2828.

13. Nieman K, Oudkerk M, Rensing B, *et al.* Coronary angiography with multi-slice computed tomography. *Lancet* 2001;357:599-603.
14. Ohnesorge B, Flohr T, Becker C, *et al.* Cardiac imaging by means of electrocardiographically gated multisection spiral CT: initial experience. *Radiology* 2000;217:564-571.
15. Haase J, Escaned J, van Swijndregt EM, *et al.* Experimental validation of geometric and densitometric coronary measurements on the new generation Cardiovascular Angiography Analysis System (CAAS II). *Cathet Cardiovasc Diagn* 1993;30:104-114.
16. Bland JM, Altman DG. Statistical methods for assessing agreement between two methods of clinical measurement. *Lancet* 1986;1:307-310.
17. Wulf J, Hadinger U, Oppitz U, *et al.* Stereotactic radiotherapy of extracranial targets: CT-simulation and accuracy of treatment in the stereotactic body frame. *Radiother Oncol* 2000;57:225-236.
18. Slager CJ, Hooghoudt TE, Serruys PW, *et al.* Quantitative assessment of regional left ventricular motion using endocardial landmarks. *J Am Coll Cardiol* 1986;7:317-326.
19. Wang Y, Vidan E, Bergman GW. Cardiac motion of coronary arteries: variability in the rest period and implications for coronary MR angiography. *Radiology* 1999;213:751-758.
20. Wong JW, Sharpe MB, Jaffray DA, *et al.* The use of active breathing control (ABC) to reduce margin for breathing motion. *Int J Radiat Oncol Biol Phys* 1999;44:911-919.

Chapter

5

Dosimetric comparison between high-precision external beam radiotherapy and endovascular brachytherapy for coronary artery in-stent restenosis

Edward M. Leter
Peter J.C.M. Nowak
Koen Nieman
Johannes P. Marijnissen
Stéphane G. Carlier
Connie de Pan
Patrick W. Serruys
Peter C. Levendag

Int J Radiat Oncol Biol Phys 2002;54:1252–1258

Oral presentation at the 2001 annual meeting of ASTRO

Abstract

Purpose: Several drawbacks of endovascular brachytherapy for the treatment of coronary artery in-stent restenosis may be addressed by high-precision external beam radiotherapy (EBRT). The dosimetric characteristics of both treatment techniques were compared.

Methods and materials: The traversed volume of 10 coronary artery stents during the cardiac cycle was determined by electrocardiographically gated multislice spiral CT in 10 patients. By use of this traversed volume, high-precision EBRT treatment plans were generated for stents in the left circumflex (LCx), left anterior descending (LAD), and right coronary artery (RCA). The maximum dose to the nontargeted major coronary arteries was determined and compared to similar data calculated for endovascular brachytherapy.

Results: High-precision EBRT targeted at LCx stents contributed a mean maximum dose (D_{\max}) of 83.5% (range 71.6–95.3%) and 16.3% to the LAD and RCA, respectively. Targeted LAD stents contributed a mean D_{\max} of 39.3% (range: 14.5–94.8%) and 5.2% (range: 0–13.4%) to the LCx and RCA, respectively. Targeted RCA stents contributed a mean D_{\max} of 6.2% (range: 0–12.4%) and 5.8% (range: 0–11.5%) to the LCx and LAD, respectively. Endovascular brachytherapy targeted at LCx stents contributed a mean D_{\max} of 1.7% (range: 0.7–2.7%) and 1.0% (range: 0.6–1.4%) to the LAD and RCA, respectively. Targeted LAD stents contributed a mean D_{\max} of 5.2% (range: 0.5–11.4%) and 0.7% (range: 0.4–1.1%) to the LCx and RCA, respectively; targeted RCA stents contributed a mean D_{\max} of 0.3% (range: 0.2–0.5%) and 0.2% (range: 0.1–0.3%) to the LCx and LAD, respectively.

Conclusions: Although the doses distributed throughout the heart were higher for high-precision EBRT compared to endovascular brachytherapy, they are expected to be clinically irrelevant when nontargeted major coronary arteries are not closely situated to the targeted vessel segment. These encouraging results warrant further investigation of high-precision EBRT as a potential alternative to endovascular brachytherapy for the treatment of coronary artery in-stent restenosis.

Introduction

Endovascular brachytherapy as an adjunct to percutaneous transluminal coronary angioplasty (PTCA) has demonstrated promising results in several randomized clinical trials for the treatment of coronary artery in-stent restenosis (1, 2). However, it is also associated with a number of drawbacks that may be addressed by external beam radiotherapy (EBRT). Dose fractionation, synchronization with cell kinetics, and improved dose homogeneity over a range of tissue depths are examples of the potential advantages EBRT offers over endovascular brachytherapy. So far, animal studies on the effects of EBRT targeted at virtually the entire heart for inhibition of coronary artery restenosis consistently reported myocardial inflammation and fibrosis (3–5). These studies reported also conflicting results with regard to neointima formation, i.e., exacerbated (4), unchanged (3), and reduced restenosis (5). Although the latter study provides evidence for the effectiveness of whole heart EBRT at 21 Gy to inhibit neointima formation in stented porcine coronary arteries, the observed cardiac tissue side effects will hamper clinical implementation of such a treatment technique. Hence, exploration of high-precision EBRT has been suggested (3, 5–7), which requires first of all a small target volume, such as a coronary artery stent. Recently, single breath hold electrocardiographically gated multislice spiral computed tomography (MSCT) was used in a successful attempt to define the volume through which coronary artery stents traverse during the cardiac cycle, as a potential target for high-precision EBRT. The stent-traversed volume (STV) during the cardiac cycle was reported to comprise only a fraction – that is, less than 0.6% – of the whole heart volume (WHV) in 8 patients (8).

The purpose of this study was to use the coronary artery STV during the cardiac cycle as a target for high-precision EBRT treatment planning and to compare the dose distributions to those obtained for endovascular brachytherapy.

Methods and materials

Patients

Imaging data for 10 patients (3 women and 7 men, ages 61 ± 8 years [mean \pm 1 standard deviation], age range: 48–75 years) who underwent clinical investigation of coronary artery in-stent restenosis by MSCT were used for this study. A single stent in one of the three major coronary arteries was studied in each patient: 2 in the left circumflex (LCx), 6 in the left anterior descending (LAD), and 2 in the right coronary artery (RCA). The implanted stents included 1 Genius (EuroCor, Bonn, Germany), 2 ACS Multi-link Duet (Guidant, Santa Clara, CA), 3 NIROYAL

(Medinol, Maple Grove, MN), 2 BX Velocity (Cordis, Warren, NJ), 1 Terumo (Terumo, Tokyo, Japan), and 1 R stent (Orbus, Ft. Lauderdale, FL). The nominal stent length was 20.9 ± 7.4 mm (range: 13–38 mm). The median interval between stent implantation and the MSCT scan was 15 days (range: 3–89 days). All patients were in sinus rhythm. The institution's ethical review board approved the study. All participants gave informed consent.

Stereotactic body frame

Patients were rigidly positioned on the couch of the MSCT scanner in a stereotactic body frame (Elekta, Crawley, West Sussex, UK) on a vacuum pillow perfectly shaped to the patient's body. Details have been described elsewhere (8, 9).

MSCT: Data acquisition

A contrast-enhanced MSCT scan (Somatom Plus 4 Volume-Zoom, Siemens AG, Forchheim, Germany) of the entire heart, using a 4×1.0 -mm collimation protocol, was performed during a single breath hold (10–12). Synchronized to the recorded electrocardiogram, transverse slices were retrospectively reconstructed on an off-line workstation (Work-in-progress Siemens Cardio Package, Siemens AG). Because the spiral CT data was acquired continuously, a stack of overlapping slices can be reconstructed at any point. Ten isocardiophasic volume datasets were created by positioning the 250-ms reconstruction window at 0%, 10%, and 20–90% of the cardiac cycle (8).

MSCT: Data analysis

The stent wall was manually contoured along the line through its center in each of the 10 MSCT datasets by using an XKnife RT 1.03 (Radionics, Burlington, MA) three-dimensional (3D) radiosurgery treatment planning system. Stent volumes were constructed by the treatment planning software. All contoured stent volumes were copied into a diastolic dataset. The volume around all 10 stent positions was encompassed as a measure of the STV during the cardiac cycle – that is, the cardiac motion effect during contraction and relaxation (8).

External beam radiotherapy dose distributions

High-precision EBRT treatment plans were generated for the traversed volume during the cardiac cycle of each coronary artery stent by use of the treatment planning system. For this purpose, the targeted stent, the remainder of the targeted coronary artery, the two nontargeted major coronary arteries, and the heart volume were contoured in the diastolic MSCT dataset. The planning target volume (PTV) was obtained by adding a 3D craniocaudal margin of 10 mm and a ventrodorsal and lateral margin

of 5 mm to account for the effect of respiration during breath hold and for setup errors. With the entire body contour taken into account, the dose was prescribed to the 80%-encompassing isodose surface, by using three noncoplanar arcs with 6-MV photons (Figure 1). First, a class solution was created that entailed one arc in the sagittal plane and two transversal arcs – with a sufficient gap to avoid overlap with the sagittal arc – using circular cones in conjunction with the jaws of the accelerator. Subsequently, by varying the weight of the arcs, the treatment plan was optimized for each patient. The plans were normalized to 100% in the isocenter. The use of arcs rather than fixed-shaped fields resulted in a higher dose falloff around the targeted volume, that is, a lesser integral dose in the surrounding critical tissues.

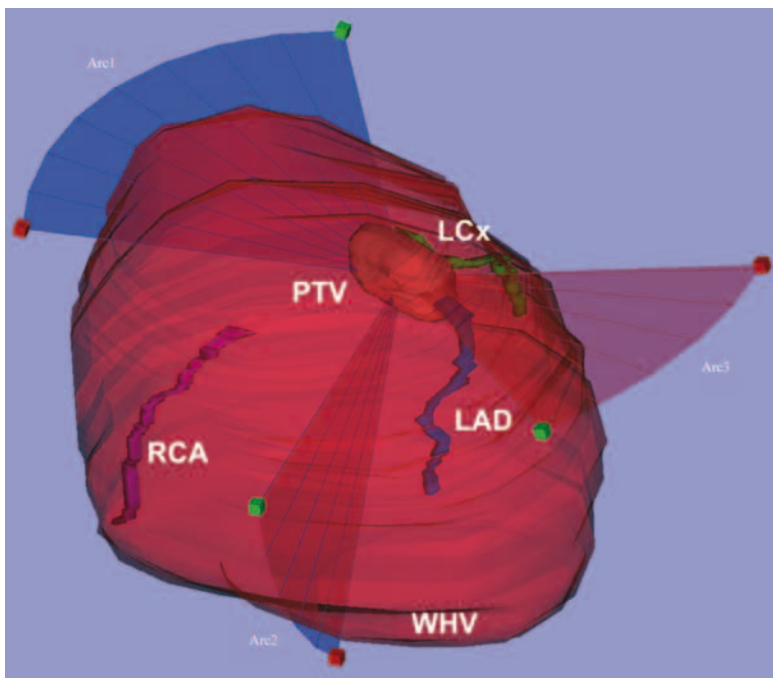


Figure 1. Anterior view on an example of a highly conformal external beam radiotherapy treatment plan for an LAD coronary artery stent. The PTV surrounding the targeted stent-traversed volume during the cardiac cycle is depicted in red within the transparent WHV. Also depicted within the WHV are the nontargeted remainder of the LAD in blue, the LCx in green, and the RCA in purple.

The volume receiving \geq the prescribed dose (V_{80}) and the volume of the nontargeted major coronary arteries receiving $\geq 50\%$ of the total dose (V_{50}) were determined. The maximum dose (D_{max}) to the two nontargeted major coronary arteries was also determined and is reported as a percentage of the total dose received by the targeted vessel.

Endovascular brachytherapy dose distributions

The maximum dose to the nontargeted major coronary arteries for endovascular brachytherapy was calculated by measurement of the shortest spatial relationship between the respective vessel segments in a diastolic MSCT dataset. A curved source with a length of 20 mm was divided into short segments 1 mm in length. Each segment was considered as a point source (P_i). The contribution of this point source to the dose rate at a point P_r , i.e., D_{p_i} , in a nontargeted major coronary artery at a distance r_i from the point source in the targeted stent is as follows (Eq. 1):

$$D_{p_i} = \frac{f \cdot A_i K_0}{r_i^2} \cdot S(r_i) \quad (1)$$

with

$$S(r_i) = \frac{\delta}{1 + \beta r_i^2} \quad (2)$$

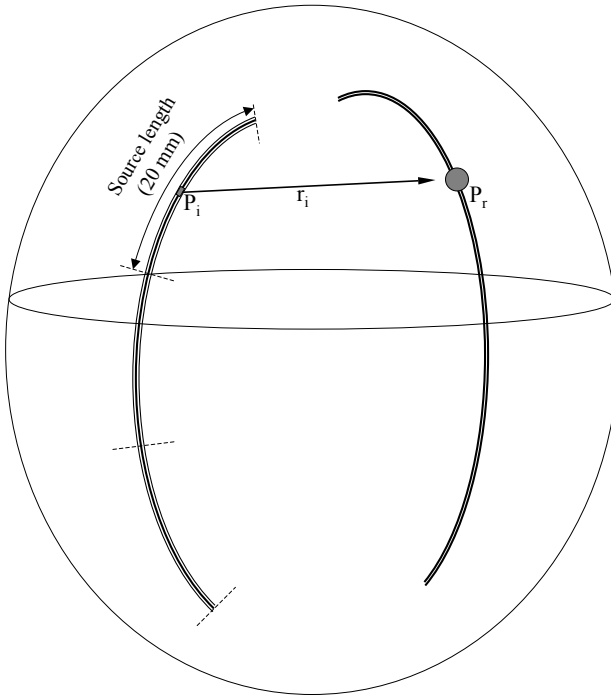


Figure 2. Diagram of the strategy to determine the maximum dose to nontargeted major coronary arteries when a stented coronary artery segment is irradiated by an endovascular iridium source.

where A_i (MBq) is the activity of the point source (1-mm segment), the conversion factor from kerma to dose in water $f = 1.1$, and the air kerma rate $K_0 = 0.10995 \mu\text{Gy/hr/MBq}$ at 1 meter distance. $S(r_i)$ describes the attenuation of the radiation by absorption and scattering with the constants $\delta = 1.018$ and $\beta = 0.6 \times 10^{-3} \text{ cm}^2$ (Eq. 2), which are applicable for iridium (13). The total dose rate in point P_r is the summed contribution of all point sources (Figure 2). The reported doses in the adjacent arteries were normalized to the reference dose of 1 Gy at 2 mm from the axis in the central plane of the assumed 20-mm total source length (14).

Results

The WHV, which was contoured as part of the high-precision EBRT treatment planning process, was $834 \pm 93 \text{ cm}^3$ (range: 665–947 cm^3). The target volume, that is, the STV during the cardiac cycle, was $1.2 \pm 1.1 \text{ cm}^3$ (range: 0.4–3.8 cm^3) and represented $\leq 0.4\%$ of the WHV in all patients. The PTV was $9.0 \pm 6.0 \text{ cm}^3$ (range: 3.9–24.2 cm^3) and represented $\leq 2.8\%$ of the WHV in all patients. A volume of $15.8 \pm 8.8 \text{ cm}^3$ (range: 5.7–35.1 cm^3) received \geq the prescribed dose when targeted by high-precision EBRT (Table 1).

Table 1. Absolute and relative high-precision external beam radiotherapy treatment planning volumes.

Patient	STV (cm^3)	PTV (cm^3)	V_{80} (cm^3)	STV/WHV (%)	PTV/WHV (%)
1	0.8	6.3	12.0	0.12	0.95
2	0.7	5.4	10.6	0.07	0.61
3	0.4	3.9	7.8	0.05	0.45
4	0.7	5.6	10.8	0.07	0.62
5	1.2	9.0	15.7	0.13	0.97
6	1.1	12.0	23.9	0.16	1.65
7	3.8	24.2	35.1	0.44	2.76
8	2.2	11.4	19.8	0.29	1.50
9	0.5	4.6	5.7	0.05	0.48
10	0.4	8.0	16.8	0.05	1.00

STV = stent traversed volume; PTV = planning target volume; V_{80} = volume receiving $\geq 80\%$ of the total dose; WHV = whole heart volume.

High-precision EBRT resulted in a V_{50} of 0 cm^3 for both nontargeted major coronary arteries for six of the targeted vessels. The two targeted LCx stents resulted in a V_{50} of 0.04 cm^3 and 0.18 cm^3 for the LAD (Patient 1 and 10, respectively), and two targeted LAD stents resulted in a V_{50} of 0.13 cm^3 and 0.04 cm^3 for the LCx (Patient 4 and 6, respectively).

High-precision EBRT targeted at LCx stents contributed a mean D_{\max} of 83.5% (range: 71.6–95.3%) and 16.3% to the LAD and RCA, respectively. Targeted LAD stents contributed a mean D_{\max} of 39.3% (range: 14.5–94.8%) and 5.2% (range: 0–13.4%) to the LCx and RCA, respectively. Targeted RCA stents contributed a mean D_{\max} of 6.2% (range: 0–12.4%) and 5.8% (range: 0–11.5%) to the LCx and LAD, respectively. Endovascular brachytherapy targeted at LCx stents contributed a mean D_{\max} of 1.7% (range: 0.7–2.7%) and 1.0% (range 0.6–1.4%) to the LAD and RCA, respectively. Targeted LAD stents contributed a mean D_{\max} of 5.2% (range: 0.5–11.4%) and 0.7% (range: 0.4–1.1%) to the LCx and RCA, respectively; targeted RCA stents contributed a mean D_{\max} of 0.3% (range: 0.2–0.5%) and 0.2% (range: 0.1–0.3%) to the LCx and LAD, respectively (Table 2).

As was anticipated, an inverse relationship between the dose received by the nontargeted major coronary arteries and their distance from the targeted coronary artery stent was observed for both high-precision EBRT and endovascular brachytherapy. High (maximum) doses in nontargeted vessels were associated with a proximal location of the targeted coronary artery stent in the LCx or LAD, i.e., segment 11 and 6 for the LCx and LAD, respectively (Table 2, Figure 3).

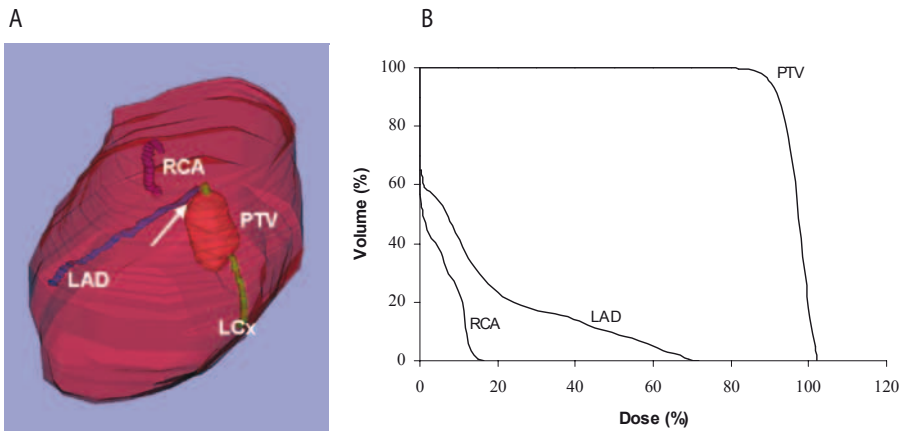


Figure 3. (a) Lateral view on a high-precision EBRT treatment plan (arcs not shown) targeting the PTV depicted in red around an LCx coronary artery stent (Patient 1) closely situated (arrow) to the LAD coronary artery depicted in blue. The nontargeted remainder of the LCx is depicted in green, and the RCA is depicted in purple. (b) The corresponding dose-volume histogram shows that a high (maximum) dose was contributed to the LAD.

Table 2. Maximum dose to nontargeted major coronary arteries as a percentage of the total dose received by the stented coronary artery segment targeted by either high-precision external beam radiotherapy or endovascular brachytherapy.

Patient	External beam radiotherapy			Endovascular brachytherapy		
	LCx	LAD	RCA	LCx	LAD	RCA
1	T.s. 11	71.6	16.3	T.s. 11	2.7	0.6
2	21.6	T.s. 7	10.4	2.7	T.s. 7	0.4
3	31.3	T.s. 7	0	2.7	T.s. 7	0.5
4	94.8	T.s. 6	0	11.4	T.s. 6	1.1
5	21.6	T.s. 7	0	5.6	T.s. 7	0.8
6	51.8	T.s. 6	7.6	8.4	T.s. 6	0.9
7	0	0	T.s. 2	0.2	0.1	T.s. 2
8	12.4	11.5	T.s. 2	0.5	0.3	T.s. 2
9	14.5	T.s. 7	13.4	0.5	T.s. 7	0.4
10	T.s. 11	95.3	16.3	T.s. 11	0.7	1.4

LCx = left circumflex; LAD = left anterior descending; RCA = right coronary artery; T.s. = targeted segment of the LCx, LAD and RCA according to the definitions on segmental anatomy by the American Heart Association (20).

Discussion

Although the doses to the nontargeted major coronary arteries were higher for high-precision EBRT compared to endovascular brachytherapy, in essence these doses are expected to be clinically irrelevant. However, high (maximum) doses were observed when a coronary artery stent targeted by high-precision EBRT was closely situated to a nontargeted major coronary artery, which applies anatomically for the proximal LCx and LAD, because they both arise from the left main coronary artery (Table 2, Figure 3). The doses in neighboring nontargeted major coronary arteries must depend also on the displacement of the targeted vessel segment during the cardiac cycle, because both the motion pattern and amplitude of coronary arteries have been reported to vary substantially from patient to patient (15). The high (maximum) doses may be prevented by additional reduction of the target volume. Because we are already dealing with a small target volume, the high (maximum) doses to nontargeted coronary arteries should be prevented preferably by patient selection, that is, exclusion of patients on the basis of treatment planning results. For all such selected patients, high-precision EBRT may pose a feasible alternative to endovascular brachytherapy for the treatment of coronary artery in-stent restenosis. The former treatment technique offers several potential advantages, such as dose fractionation and flexibility to optimize the time of treatment in relation to

target cell proliferation after PTCA. Whether these and other advantages of high-precision EBRT, such as improved dose homogeneity over a range of tissue depths, outweigh procedural complexity and duration remains to be established.

High-precision EBRT targeted at the STV during the cardiac cycle would substantially reduce the target volume in comparison to previous studies on EBRT targeted at virtually the entire heart. Schwartz *et al.* (4), for instance, reported a small increase of neointimal hyperplasia after a single or fractionated dose of 4–8 Gy targeted at virtually the whole porcine heart. Myocardial fibrosis was also observed. Marijianowski *et al.* (3) reported no effect on neointimal hyperplasia after a single dose of 14 Gy targeted at the porcine heart; however, interstitial and perivascular fibrosis in the myocardium was observed. Because the whole heart received the prescribed dose, the authors argued that the side effects might be related to the irradiation technique. Recently Verheije *et al.* (5) reported reduced neointimal hyperplasia after a single dose of 21 Gy targeted at the whole porcine heart, but also incomplete re-endothelialization, as well as myocardial inflammation and fibrosis. The latter study provides evidence for the effectiveness of EBRT in preventing coronary artery in-stent restenosis. However, clinical implementation demands the prevention of side effects, which may be achieved by the application of high-precision EBRT. Similar to whole-heart EBRT, high-precision EBRT will need to be investigated in an animal model after its technical feasibility has been further refined. Exploration of high-precision EBRT may also be of use for the treatment of arterial venous bridge fistula, because recent data suggests that high, single radiation doses, i.e., ≥ 15 Gy, are needed to induce significant inhibition of neointimal proliferation (16).

The STV is a measure mainly of the cardiac motion effect on coronary artery stent position throughout the cardiac cycle, because MSCT was performed during one breath hold. However, the position of a stent throughout the cardiac cycle is also greatly affected by respiratory motion. Because a minimal target volume is of the utmost importance, the respiratory motion effect may best be countered similarly to the way MSCT was performed, that is, during breath hold. This can be achieved by, for instance, the use of active breathing control, which allows temporary and reproducible immobilization of internal thoracic structures (17). The 3D PTV margin by which the STV was encompassed is anticipated to be adequate when high-precision EBRT treatment planning and treatment would be performed by use of active breathing control. The margin was derived from clinical experience with stereotactic radiotherapy of extracranial targets (9, 18) and has been shown to be adequate for lung and liver cancers when breathing mobility is reduced to 5 mm by applying mechanical abdominal pressure (19).

A shortcoming of this study relates to the fact that the dose distributions throughout the heart, both for high-precision EBRT and endovascular brachytherapy, were determined by use of a single diastolic MSCT dataset. As a result, the dynamic relationships among the different coronary arteries during the cardiac cycle were not dosimetrically accounted for; however, a significant effect should not be expected.

Although the doses distributed throughout the heart were higher for high-precision EBRT compared to endovascular brachytherapy, these doses are expected to be clinically irrelevant when nontargeted major coronary arteries are not closely situated to the targeted vessel segment. These encouraging preliminary results warrant further investigation of high-precision EBRT as a potential alternative to endovascular brachytherapy for the treatment of coronary artery in-stent restenosis.

References

1. Leon MB, Teirstein PS, Moses JW, *et al.* Localized intracoronary gamma-radiation therapy to inhibit the recurrence of restenosis after stenting. *N Engl J Med* 2001;344:250-256.
2. Verin V, Popowski Y, de Bruyne B, *et al.* Endoluminal beta-radiation therapy for the prevention of coronary restenosis after balloon angioplasty. The Dose-Finding Study Group. *N Engl J Med* 2001;344:243-249.
3. Marijianowski MM, Crocker IR, Styles T, *et al.* Fibrocellular tissue responses to endovascular and external beam irradiation in the porcine model of restenosis. *Int J Radiat Oncol Biol Phys* 1999;44:633-641.
4. Schwartz RS, Koval TM, Edwards WD, *et al.* Effect of external beam irradiation on neointimal hyperplasia after experimental coronary artery injury. *J Am Coll Cardiol* 1992;19:1106-1113.
5. Verheye S, Coussement PK, Salame MY, *et al.* High-dose external beam irradiation inhibits neointima formation in stented pig coronary arteries. *Int J Radiat Oncol Biol Phys* 2001;51:820-827.
6. Farber LA, Bloch P, Yorke ED, *et al.* A dosimetric comparison of conventional vs conformal external beam irradiation of a stented coronary artery utilizing a new fluoroscopic imaging detector system. *Cardiovasc Radiat Med* 1999;1:80-85.
7. Mazur W, Kaluza GL, Raizner AE. Radiation for the treatment of restenosis. In: Tripuraneni P, Jani S, Minar E, Leon M, editors. *Intravascular brachytherapy. From theory to practice*. First ed. London: ReMEDICA Publishing Limited; 2001. p. 167-187.
8. Leter EM, Nowak PJ, Nieman K, *et al.* Definition of a moving gross target volume for stereotactic radiation therapy of stented coronary arteries. *Int J Radiat Oncol Biol Phys* 2002;52:560-565.
9. Lax I, Blomgren H, Larson D, *et al.* Extracranial stereotactic radiosurgery of localized targets. *J Radiosurg* 1998;1:135-148.
10. Achenbach S, Ulzheimer S, Baum U, *et al.* Noninvasive coronary angiography by retrospectively ECG-gated multislice spiral CT. *Circulation* 2000;102:2823-2828.
11. Nieman K, Oudkerk M, Rensing B, *et al.* Coronary angiography with multi-slice computed tomography. *Lancet* 2001;357:599-603.
12. Ohnesorge B, Flohr T, Becker C, *et al.* Cardiac imaging by means of electrocardiographically gated multisection spiral CT: initial experience. *Radiology* 2000;217:564-571.

13. Thomadsen BR, Houdek PV, van der Laarse R, *et al.* Treatment planning and optimization. In: Nag S, editor. High dose rate brachytherapy: A textbook. Armonk, NY: Futura Publishing Company; 1994. p. 79-145.
14. Potter R, Van Limbergen E, Dries W, *et al.* Recommendations of the EVA GEC ESTRO Working Group: prescribing, recording, and reporting in endovascular brachytherapy. Quality assurance, equipment, personnel and education. *Radiother Oncol* 2001;59:339-360.
15. Wang Y, Vidan E, Bergman GW. Cardiac motion of coronary arteries: variability in the rest period and implications for coronary MR angiography. *Radiology* 1999;213:751-758.
16. Williams JP, Illig KA, Hernady EB, *et al.* Results of a large animal study examining the effects of external beam irradiation on the inhibition of intimal hyperplasia in a prosthetic arterial bypass model at 1 and 3 months [abstract]. *Int J Radiat Oncol Biol Phys* 2001;51:146.
17. Wong JW, Sharpe MB, Jaffray DA, *et al.* The use of active breathing control (ABC) to reduce margin for breathing motion. *Int J Radiat Oncol Biol Phys* 1999;44:911-919.
18. Wulf J, Hadinger U, Oppitz U, *et al.* Stereotactic radiotherapy of extracranial targets: CT-simulation and accuracy of treatment in the stereotactic body frame. *Radiother Oncol* 2000;57:225-236.
19. Haedinger U, Wulf J, Oppitz U, *et al.* Extracranial stereotactic radiotherapy: Evaluation of the PTV to compensate target mobility and set-up inaccuracy over the complete target volume measured by DVH from repeated CT-simulation [abstract]. *Int J Radiat Oncol Biol Phys* 2001;51:45-46.
20. Austen WG, Edwards JE, Frye RL, *et al.* A reporting system on patients evaluated for coronary artery disease. Report of the Ad Hoc Committee for Grading of Coronary Artery Disease, Council on Cardiovascular Surgery, American Heart Association. *Circulation* 1975;51:5-40.

Chapter

6

Three-dimensional lung tumor displacements throughout consecutive respiratory cycles determined by multislice spiral computed tomography

Edward M. Leter
Filippo Cademartiri
Peter C. Levendag
Thomas Flohr
Henk Stam
Peter J. Nowak

Submitted for publication

Abstract

Eight patients with 12 lung tumors were scanned using respiratory-gated multislice spiral computed tomography (MSCT). In each patient 10 datasets equally distributed throughout consecutive respiratory cycles were retrospectively reconstructed from the acquired MSCT data. The tumors were contoured in each dataset. By three-dimensional matching of the 10 target volumes, lung tumor center of mass displacements throughout the consecutive respiratory cycles could be determined for each patient. Respiratory-gated MSCT can therefore be of use for conformal radiotherapy treatment planning imaging.

Introduction

The use of computed tomography (CT) imaging is essential for conformal radiotherapy treatment planning. In common clinical practice these CT scans are performed while the patient breathes freely. Thoracic and abdominal tumors can move as much as 35 millimeters with breathing (1). Because the CT scanners commonly applied for radiotherapy treatment planning are not designed to determine respiratory motion, the clinical target volume is encompassed by an empirical generalized margin to account for this periodic physiological motion effect. However, individualized margins, as opposed to generalized margins, are required for radiation treatment of target volumes affected by respiratory motion (2). With the introduction of multislice spiral computed tomography (MSCT) individualized determination of periodic physiological target volume motion has come within reach. These scanners permit high-speed scanning with a high in-plane and craniocaudal resolution (3). Leter *et al.* (4) described one of the first applications of MSCT within the field of radiotherapy. These authors used MSCT scans gated to the electrocardiogram (ECG) to define a potential radiotherapy target volume. The purpose of this study was to test whether the strategy described in the latter study could be applied for determination of respiratory lung tumor motion.

Materials and methods

Eight patients (6 men, 2 women; mean age, 55.5 years; age range, 46-65 years) with 12 lung metastases, scheduled for a diagnostic thoracic CT, were included in this study. They were asked to participate by their referring physician. The University Hospital Ethical Review Board approved this study. All participants gave written informed consent.

Thoracic MSCT of the entire lung volume was performed using a 16-slice scanner (Sensation 16, Siemens, Forchheim, Germany) which provided a temporal resolution of 250 ms. The scanner allowed for the following parameters: 0.5-s rotation time, temporal resolution 250 ms (180° reconstruction algorithm), detector collimation 16 x 1.5 mm, table feed 3.6 mm/rotation, tube voltage 120 kV and current 150 mAs. The smallest pitch (table feed per rotation divided by the collimated width of the entire detector) the scanner allowed for at the time of the study was: 0.15.

During the scan patients were instructed to breath through a spirometer (MasterScope Color, Viasys Healthcare, Bilthoven, The Netherlands), connected to a laptop computer, and were fitted with a nose clip to prevent air leakage through the nostrils. To ensure multiphase detection of respiratory tumor motion without data

loss, the breathing cycles had to be limited to about 3 seconds. Audio prompting was used to optimize breathing regularity, i.e., the patient was instructed to perform inspiration and expiration at the 48 ticks per minute of a metronome.

Because the spiral CT data was acquired continuously, a stack of overlapping slices can be reconstructed at any time point. For each patient ten stacks of 1.5 mm slices were reconstructed equally distributed throughout consecutive respiratory cycles by dedicated S16-SpiroRecon work-in-progress software (Siemens, Forchheim, Germany) from the acquired MSCT data on an off-line workstation. For this purpose the 250 ms reconstruction window was positioned from 0 to 100% of the respiratory cycles with 10% increments. The lung tumors were manually contoured at a window of 1500 Hounsfield units and a level of -500 Hounsfield units in all 10 MSCT datasets of each patient using a custom-made tumor contouring and matching software program (Rotterdam, The Netherlands) developed by one of the authors (P.J.N.). An end-inspiratory tumor volume was selected as a reference and was consecutively matched by three-dimensional (3D) translation and rotation with the other nine volumes to determine the lung tumor center of mass displacements throughout the consecutive respiratory cycles.

Results

All patients could cooperate with the breathing procedure. There was no exclusion of patients during the study period. The complete imaging procedure took 15 minutes in the first 2 patients and was finished within 10 minutes in the remaining patients. The scan time was 43.7 ± 3.1 seconds (mean \pm 1 standard deviation). The acquired imaging data provided adequate image quality for multiphase visualization of lung tumors.

The mean reference tumor volume was $2.2 \text{ cm}^3 \pm 17.3 \text{ cm}^3$. The mean of the maximum 3D center of mass displacements between any two phases during the consecutive respiratory cycles for all 12 lung tumors are summarized in the Table. The maximum amplitude in the lateral direction was 2.2 ± 1.0 mm, 3.3 ± 1.4 mm in the ventrodorsal direction and 13.3 ± 7.4 mm in the craniocaudal direction.

Table. Tumor locations and maximum amplitudes in the lateral (L), ventrodorsal (VD) and craniocaudal (CC) direction.

Patient	Tumor location	Maximum amplitude of motion (mm)		
		L	VD	CC
1	Upper lobe	1.2	2.9	8.0
2	Upper lobe	2.2	2.2	4.1
3A	Lower lobe	3.1	5.5	20.8
3B	Lower lobe	2.4	1.8	19.8
3C	Upper lobe	1.9	4.7	7.5
3D	Upper lobe	1.2	2.7	2.9
4	Lower lobe	2.9	3.7	14.4
5	Lower lobe	1.9	3.2	26.1
6A	Lower lobe	1.9	5.8	15.0
6B	Lower lobe	3.0	2.4	19.5
7	Upper lobe	4.5	3.0	6.6
8	Lower lobe	0.6	1.5	15.0

Discussion

It has recently been described how an ECG-gated MSCT imaging strategy could be used to determine cardiac motion of a potential radiotherapy target volume. The strategy entailed retrospective reconstruction of MSCT data during 10 selected phases equally distributed throughout the RR-interval of consecutive cardiac cycles. By the consideration of the fourth dimension, namely time, cardiac target volume motion could be determined (4). Our current results represent a successful application of this strategy for determination of respiratory lung tumor motion. The strategy allows individualized determination of margins to account for respiratory motion of any thoracic or abdominal target volume during treatment planning imaging. A method for obtaining such four-dimensional (4D) datasets of lung tumors has been described previously by Low *et al.* (5). These authors used sequential MSCT scans. We chose a less laborious strategy by spiral scans. Moreover, because our data was reconstructed relative to the scan start point, in principle the only requirement is a breathing motion measure that provides a clear start and end point of the respiratory cycle.

The observed maximum motion amplitudes and the tendency of greater motion in the lower lobes (Table) concur with previous reports on respiratory motion of lung tumors (6, 7). Because of the small number of patients we could not provide motion data for the different lung lobes separately.

Because of pitch limitations at the time of the study the duration of the respiratory cycles had to be limited to a maximum of 3 seconds. A lower pitch value is expected to be available in the near future.

In conclusion, 4D MSCT datasets allowed determination of respiratory lung tumor displacements throughout consecutive respiratory cycles. The acquisition of such 4D spiral imaging datasets for radiotherapy purposes and their reproducibility warrants further investigation.

Acknowledgements

We thank Harold Smeets of Viasys Healthcare The Netherlands for providing us with a spirometer for the study and Edward Donkersloot for his technical support.

References

1. Ozhasoglu C, Murphy MJ. Issues in respiratory motion compensation during external-beam radiotherapy. *Int J Radiat Oncol Biol Phys* 2002;52:1389-1399.
2. Stevens CW, Munden RF, Forster KM, *et al.* Respiratory-driven lung tumor motion is independent of tumor size, tumor location, and pulmonary function. *Int J Radiat Oncol Biol Phys* 2001;51:62-68.
3. Nieman K, Oudkerk M, Rensing B, *et al.* Coronary angiography with multi-slice computed tomography. *Lancet* 2001;357:599-603.
4. Leter EM, Nowak PJ, Nieman K, *et al.* Definition of a moving gross target volume for stereotactic radiation therapy of stented coronary arteries. *Int J Radiat Oncol Biol Phys* 2002;52:560-565.
5. Low DA, Nystrom M, Kalinin E, *et al.* A method for the reconstruction of four-dimensional synchronized CT scans acquired during free breathing. *Med Phys* 2003;30:1254-1263.
6. Ekberg L, Holmberg O, Wittgren L, *et al.* What margins should be added to the clinical target volume in radiotherapy treatment planning for lung cancer? *Radiother Oncol* 1998;48:71-77.
7. Seppenwoolde Y, Shirato H, Kitamura K, *et al.* Precise and real-time measurement of 3D tumor motion in lung due to breathing and heartbeat, measured during radiotherapy. *Int J Radiat Oncol Biol Phys* 2002;53:822-834.

Chapter

7

Four-dimensional multislice spiral computed tomography for determination of respiratory lung tumor motion in conformal radiotherapy

Edward M. Leter
Filippo Cademartiri
Peter C. Levendag
Thomas Flohr
Henk Stam
Peter J. Nowak

Submitted for publication

Abstract

Purpose: We used four-dimensional multislice spiral computed tomography (MSCT) to determine respiratory lung tumor motion and compared this strategy to common clinical practice in conformal radiotherapy treatment planning imaging.

Methods and materials: The entire lung volume of 10 consecutive patients with 14 lung metastases was scanned by a 16-slice MSCT. During the scan patients were instructed to breath through a spirometer that was connected to a laptop computer. For each patient 10 stacks of 1.5 mm slices were reconstructed equally distributed throughout the respiratory cycle from the acquired MSCT data. The lung tumors were manually contoured in each dataset. For each patient the tumor volume contours of all datasets were copied to one reference dataset, which allowed determination of the volume that encompassed all 10 lung tumor positions, i.e., the tumor traversed volume (TTV) during the respiratory cycle. The TTV was compared to the 10 tumor volumes contoured for each patient to which an empirical respiratory motion margin was added. The latter target volumes were designated internal motion included tumor volume (IMITV).

Results: The TTV measurements were significantly smaller than the reference IMITV measurements. In one patient all 10 IMITVs completely encompassed the TTV. In the remaining nine patients some of the 10 IMITVs completely encompassed the TTV and some did not show overlap with up to 35% of the TTV.

Conclusions: We found that individualized determination of respiratory lung tumor motion by four-dimensional respiratory-gated MSCT represents a better and simple strategy to incorporate periodic physiological motion compared to a generalized approach. The former strategy can therefore improve common and state-of-the-art clinical practice in conformal radiotherapy.

Introduction

Conformal radiotherapy (CRT) heavily depends on adequate imaging to allow accurate treatment planning for which computed tomography (CT) scans are required. During radiation treatment of thoracic and abdominal tumors physiological motion needs to be considered. Respiratory motion in particular and also cardiac motion are the main contributors to physiological motion within the treatment session (1). Because radiotherapy becomes increasingly conformal, the issue of respiratory and cardiac tumor motion becomes increasingly important (2). However, the single-slice CT scanners installed in most radiotherapy treatment planning units are not equipped to determine these periodic physiological motion effects. By use of these scanners the tumor volume is scanned at a random time point within the respiratory cycle under the assumption that the scan images represent the average position of the tumor, i.e., midway between inspiration and expiration. To account for periodic physiological motion in common clinical practice a generalized empirical 3D margin is subsequently added to the tumor volume. Alternatively, tumor motion can be determined as part of the treatment planning procedure for which fluoroscopy is most widely used. However, tumors are often poorly visualized by use of this imaging modality. In addition, determination of actual tumor motion is technically challenging by fluoroscopy and the data cannot directly be related to the treatment planning CT data.

With the introduction of multislice spiral computed tomography (MSCT) scanners individualized determination of periodic physiological motion has come within reach. These scanners operate at an increased rotation rate and produce up to 64 slices simultaneously as opposed to single-slice CT scanners and thereby permit high-speed scanning of large volumes with a high in-plane resolution, as well as an improved craniocaudal resolution and a substantial improvement in the inter-slice correlation (3). It is for these reasons MSCT scanners allow the addition of the fourth dimension, that is, time, to the 3D treatment planning imaging process. It has been reported, for instance, that MSCT gated to the electrocardiogram allows for determination of cardiac motion of a potential thoracic high-precision conformal radiotherapy target volume (4).

Adapted from the latter study we used four-dimensional (4D) MSCT to determine respiratory lung tumor motion and compared this strategy to common clinical practice in CRT treatment planning imaging.

Methods and materials

Ten consecutive patients (8 men, 2 women; mean age, 58.0 years; age range, 46-73 years) with 14 lung metastases scheduled for diagnostic thoracic CT examination were scanned. The University Hospital Ethical Review Board approved this study and all participants gave written informed consent.

Thoracic MSCT of the entire lung volume was performed by use of a 16-slice scanner (Sensation 16, Siemens, Forchheim, Germany) which provided a temporal resolution of 250 ms. The scanner allowed for the following parameters: 0.5-s rotation time, temporal resolution 250 ms (180° reconstruction algorithm), detector collimation 16 x 1.5 mm, table feed 3.6 mm/rotation, tube voltage 120 kV and current 150 mAs. The smallest pitch (table feed per rotation divided by the collimated width of the entire detector) the scanner allowed for at the time of the study was: 0.15.

During the scan patients were instructed to breath through a spirometer (MasterScope Color, Viasys Healthcare, Bilthoven, The Netherlands), connected to a laptop computer, and were fitted with a nose clip to prevent air leakage through the nostrils. At the time of the study respiratory-gating could only be performed manually. To ensure multiphase detection of respiratory tumor motion without data loss, the breathing cycle had to be limited to about 3 seconds. With a table feed of 7.2 mm per second every z-position of the patient is registered by a detector slice for about 3 s (detector width 24 mm, $3 \times 7.2 \text{ mm} = 21.6 \text{ mm}$). Consequently, at every z-position data of an entire respiratory cycle is registered. Audio prompting was used to optimize breathing regularity, i.e., the patient was instructed to perform inspiration and expiration at the 48 ticks per minute of a metronome. Therefore the frequency of respiration ranged around 24 per minute.

Because the spiral CT data was acquired continuously, a stack of overlapping slices can be reconstructed at any time point. For each patient ten stacks of 1.5 mm slices were reconstructed equally distributed throughout the respiratory cycle by dedicated S16-SpiroRecon work-in-progress software (Siemens, Forchheim, Germany) from the acquired MSCT data on an off-line workstation. For this purpose the 250 ms reconstruction window was positioned from 0 to 100% of the respiratory cycle with 10% increments (Figure 1).

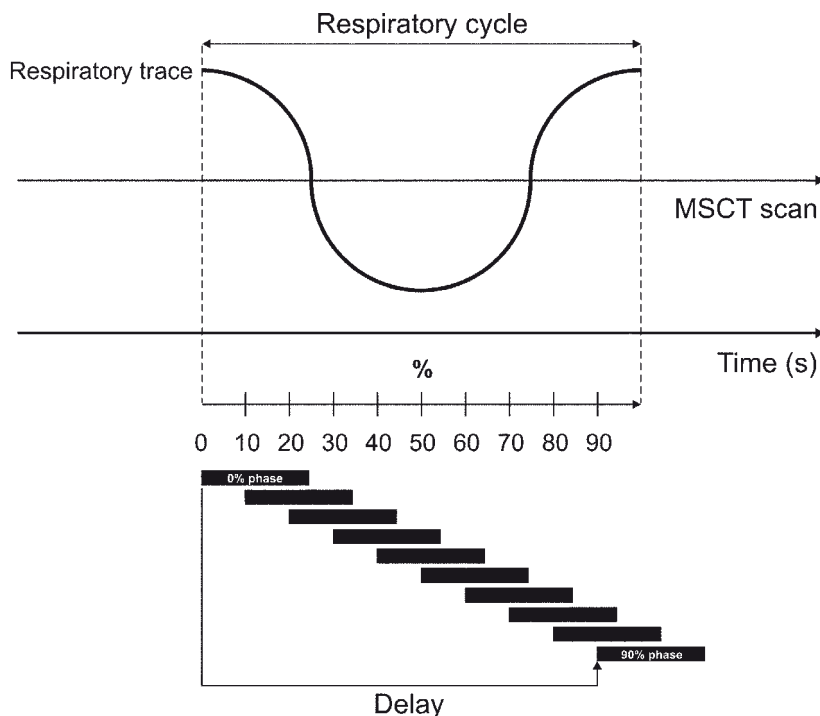


Figure 1. Diagram of the strategy for retrospective reconstruction of 10 multislice spiral computed tomography (MSCT) image datasets equally distributed throughout the respiratory cycle.

The lung tumors were manually contoured at a window of 1500 Hounsfield units and a level of -500 Hounsfield units in all 10 MSCT datasets of each patient by use of a custom-made tumor contouring software program (Rotterdam, The Netherlands) developed by one of the authors (P.J.N.). An end-inspiratory tumor volume was selected as a reference. For each patient the tumor volume contours of all datasets were copied to the reference dataset, which allowed determination of the volume that encompassed all 10 lung tumor positions, i.e., the tumor traversed volume (TTV) during the respiratory cycle. The TTV was compared to the 10 tumor volumes contoured for each patient to which an empirical 0.5 cm transversal and 1 cm craniocaudal margin for lower lobe tumors and a symmetrical 3D 0.5 cm margin for upper lobe tumors was added. The latter target volumes were designated internal motion included tumor volume (IMITV), each of which could represent a randomly scanned target volume during the respiratory cycle (Figure 2). The empirical margins around these tumor volumes were considered to be adequate on the basis of respiratory motion data reported by Seppenwoolde *et al.* (5) who studied 3D marker motion implanted in or near lung neoplasms by a real-time tumor tracking system using two fluoroscopy image processor units.

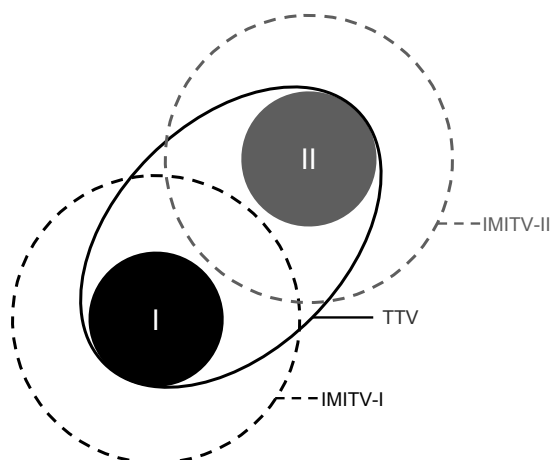


Figure 2. Diagram shows the difference between four-dimensional respiratory-gated lung tumor definition and common clinical practice in conformal radiotherapy, i.e., a tumor scanned at a random time point and encompassed by a generalized empirical respiratory motion margin. For clarity only two tumor positions (I, II) are depicted within the tumor traversed volume (TTV) during the respiratory cycle. The corresponding internal motion included tumor volumes (IMITVs) for the two tumor positions are also depicted.

The paired t test was used to test the difference between the TTV and reference IMITV measurements. A value of $P < 0.05$ was considered significant.

Results

The complete imaging procedure took 10-15 minutes and was performed successfully and without complications in all patients. The scan time was 42.9 ± 3.0 seconds (mean ± 1 standard deviation). Respiratory-gated MSCT provided adequate image quality for multiphase visualization of lung tumors (Figure 3). Seven tumors were situated in the upper lobe and the remaining seven in the lower lung lobe. None of the neoplasms was attached to surrounding rigid structures.

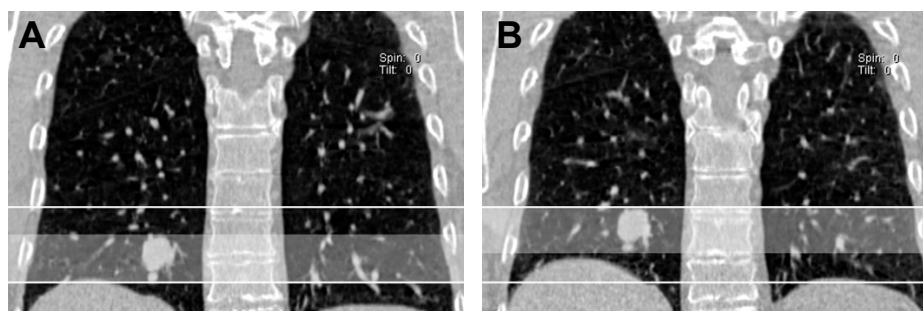


Figure 3. Example of two four-dimensional respiratory-gated multislice spiral computed tomography volumes with a coronal plane at different time points (A, B) within the respiratory cycle. The corresponding positions of the right lower lobe lung tumor are shown.

The mean reference tumor volume was $2.5 \pm 16.9 \text{ cm}^3$. The TTV measurements were significantly smaller than the reference IMITV measurements. In one patient all 10 IMITVs completely encompassed the TTV. In the remaining nine patients some of the 10 IMITVs completely encompassed the TTV and some showed an incomplete overlap with the TTV of up to 35%.

Discussion

This study shows to what extent a generalized empirical margin around a thoracic target volume to account for respiratory motion, can be arbitrary for the individual patient. We found a geometrical discrepancy between the IMITVs and the corresponding TTV in all patients. This discrepancy is partly explained by the difference in size between the respective target volumes, which could result in unnecessary dose to healthy tissue. However, when the tumor is scanned at a random time point within the respiratory cycle it is possible that a tumor position at the boundaries of the TTV is used for treatment planning (Figure 2). This partly also explains our findings because some of the IMITVs in nine patients did not show overlap with up to 35% of the TTV. Treatment planning on the basis of such a tumor position could not only result in unnecessary dose to healthy tissue but also inadequate dose to the target. Moreover, the empirical margins used in this study are far from an overestimation of the extent of respiratory motion, particularly in the craniocaudal direction for lower lobe tumors (5). Individualized determination of respiratory motion by 4D MSCT for CRT treatment planning therefore represents a better and simple strategy to incorporate periodic physiological motion of lung tumors compared to a generalized approach and can allow improvement of the

therapeutic ratio. However, such a 4D imaging strategy will demand an additional margin for microscopic extension and other treatment uncertainties.

Although the reduction of the respiratory motion effect 4D respiratory-gated MSCT allows for may be limited in comparison to novel treatment techniques such as triggered high-precision CRT (6), tumor tracking (7) and breath-holding techniques (8, 9), the difference may not necessarily reflect clinical relevance. Irradiation of the TTV may therefore represent the best trade-off between the therapeutic ratio and technical and logistic efforts. Nevertheless, 4D respiratory-gated MSCT will be useful for the afore-mentioned novel treatment techniques, e.g., to determine residual breathing motion when active and passive breath-hold techniques are applied, to identify the respiratory phase of minimal tumor motion for each patient individually and to determine residual motion within this interval for triggered high-precision CRT, and to provide the basis for 4D tumor tracking radiotherapy planning and delivery. Moreover, 4D MSCT is applicable for abdominal and pelvic target volumes and simultaneous determination of cardiac motion by additional ECG-gating is anticipated to be feasible.

Alternative methods have been described for obtaining 4D datasets. Ford *et al.* (10) and Vedam *et al.* (11) used a single-slice CT scanner to acquire a 4D dataset of a motion target phantom. The latter authors also scanned a lung cancer patient. The spatial and temporal resolution was limited in both studies inherent to the use of a single-slice CT scanner. Low *et al.* (12) used a four-slice MSCT scanner in the cine mode to acquire 15 scans at 23-26 successive couch positions for a 4D image dataset of the entire thorax in three lung cancer patients. In the light of the specifications of the latest generation of MSCT scanners, we chose for a different, simpler and less time-consuming strategy to acquire 4D respiratory-gated image datasets adapted from the previously described strategy to determine cardiac motion of a potential high-precision CRT thoracic target volume (4).

Because of the specifications of the MSCT scanner at the time of the study, the duration of the respiratory cycle had to be limited to about 3 seconds. An improvement of these specifications is expected to be available in the near future and will allow patients to breath at their normal frequency during 4D respiratory-gated MSCT scans.

Because the frequency and amplitude of respiration varies over time (2) it is important for any application of 4D respiratory-gated MSCT to establish whether target volume determination is reproducible over time. Although not the subject of the current study it seems a fair anticipation that the TTV will be more representative over time than the IMITV because the random acquisition of the latter results in additional uncertainty compared to the former. Training patients to improve breathing regularity using audio prompting to the breathing frequency

and visual feedback of the respiratory trace (13) will be of paramount importance for radiotherapy on the basis of 4D respiratory-gated MSCT. During our study respiratory-gating was performed manually. This did not represent a problem because data was reconstructed relative to the scan start point. It is for this reason also that definition of the TTV does not demand spirometry, i.e., in principle the only requirement is a breathing motion measure that provides a clear start and end point of the respiratory cycle.

Although our findings are preliminary they strongly suggest that 4D respiratory-gated MSCT can improve common and state-of-the-art clinical practice in CRT. Future study is warranted to further explore the advantages MSCT offers for high-precision CRT including combinations with other imaging modalities, e.g., magnetic resonance imaging or positron emission tomography, and efficient strategies to facilitate treatment planning of 4D image datasets.

Acknowledgments

We thank Harold Smeets of Viasys Healthcare The Netherlands for providing us with a spirometer for the study and Edward Donkersloot for his technical support.

References

1. Langen KM, Jones DT. Organ motion and its management. *Int J Radiat Oncol Biol Phys* 2001;50:265-278.
2. Ozhasoglu C, Murphy MJ. Issues in respiratory motion compensation during external-beam radiotherapy. *Int J Radiat Oncol Biol Phys* 2002;52:1389-1399.
3. Nieman K, Oudkerk M, Rensing B, *et al.* Coronary angiography with multi-slice computed tomography. *Lancet* 2001;357:599-603.
4. Leter EM, Nowak PJ, Nieman K, *et al.* Definition of a moving gross target volume for stereotactic radiation therapy of stented coronary arteries. *Int J Radiat Oncol Biol Phys* 2002;52:560-565.
5. Seppenwoolde Y, Shirato H, Kitamura K, *et al.* Precise and real-time measurement of 3D tumor motion in lung due to breathing and heartbeat, measured during radiotherapy. *Int J Radiat Oncol Biol Phys* 2002;53:822-834.
6. Kubo HD, Len PM, Minohara S, *et al.* Breathing-synchronized radiotherapy program at the University of California Davis Cancer Center. *Med Phys* 2000;27:346-353.
7. Shirato H, Shimizu S, Kitamura K, *et al.* Four-dimensional treatment planning and fluoroscopic real-time tumor tracking radiotherapy for moving tumor. *Int J Radiat Oncol Biol Phys* 2000;48:435-442.
8. Rosenzweig KE, Hanley J, Mah D, *et al.* The deep inspiration breath-hold technique in the treatment of inoperable non-small-cell lung cancer. *Int J Radiat Oncol Biol Phys* 2000;48:81-87.
9. Wong JW, Sharpe MB, Jaffray DA, *et al.* The use of active breathing control (ABC) to reduce margin for breathing motion. *Int J Radiat Oncol Biol Phys* 1999;44:911-919.
10. Ford EC, Mageras GS, Yorke E, *et al.* Respiration-correlated spiral CT: a method of measuring respiratory-induced anatomic motion for radiation treatment planning. *Med Phys* 2003;30:88-97.
11. Vedam SS, Keall PJ, Kini VR, *et al.* Acquiring a four-dimensional computed tomography dataset using an external respiratory signal. *Phys Med Biol* 2003;48:45-62.
12. Low DA, Nystrom M, Kalinin E, *et al.* A method for the reconstruction of four-dimensional synchronized CT scans acquired during free breathing. *Med Phys* 2003;30:1254-1263.
13. Kini VR, Vedam SS, Keall PJ, *et al.* Patient training in respiratory-gated radiotherapy. *Med Dosim* 2003;28:7-11.

Chapter

8

Summary and conclusions

Due to technological developments, the conformality of external beam radiotherapy (EBRT) has increased substantially. Hence, there is a growing need to accurately account for geometrical uncertainties such as organ motion and patient and beam set-up deviations. Respiratory and cardiac motion are the main contributors to intra-fraction positional variations of thoracic and abdominal target volumes. This thesis describes the development of strategies to deal with these periodic physiological motion effects for each patient individually. State-of-the-art imaging techniques have been used to better account for the fourth dimension, namely time, in the 3D CRT process.

Biplane angiography to determine and incorporate cardiac target volume motion

Intravascular brachytherapy is an effective treatment for the prevention of coronary artery de novo and in-stent restenosis. However, intravascular brachytherapy suffers from several radiobiological, clinical, physical and logistic disadvantages that may be circumvented by the use of an EBRT technique. Embedded in the general aim of this thesis, investigation of the clinical feasibility of CRT for the prevention of coronary artery in-stent restenosis, as an alternative to intravascular brachytherapy, represented an excellent study model. In **chapter 2** it is demonstrated that 3D reconstructions derived from biplane angiograms synchronized to the electrocardiogram (ECG) can be used to accurately determine the volume through which a coronary artery stent traverses during the cardiac cycle. This volume, less than 0.8% of the whole heart volume, represents a potential target volume for CRT. In **chapter 3** it is established that the coronary artery stent traversed volume (STV), as determined by ECG-synchronized biplane angiograms, can be reduced significantly when defined during the systole, diastole or 160–480 ms intervals within the cardiac cycle.

Because biplane X-ray imaging data are not directly compatible with EBRT treatment planning systems, it was attempted to apply the afore-mentioned strategy using CT scans.

MSCT to determine and incorporate cardiac target volume motion

CT scanners commonly applied for radiotherapy treatment planning are not designed to determine respiratory and cardiac motion. With the introduction of MSCT scanners, the afore-mentioned limitation can be overcome. In **chapter 4**, the 3D positional variation of coronary artery stents in patients immobilized in a stereotactic body frame was studied by single-breath hold ECG-gated MSCT. Reconstructions were acquired for 10 retrospectively selected phases equally distributed throughout the R-R interval of the cardiac cycle. The volume encompassing all 3D positions of a stent could be determined as a measure of the STV during the cardiac cycle. The

STV represented less than 0.6% of the whole heart volume in the studied patients. **Chapter 5** describes the results of a dosimetric comparison between intravascular brachytherapy targeted at a stented coronary artery segment, and EBRT targeted at the STV during the cardiac cycle as determined by ECG-gated MSCT. An EBRT treatment plan was created for stents in the left circumflex (LCx), left anterior descending (LAD), and right coronary artery (RCA). The doses distributed throughout the heart were higher for EBRT. However, these increased doses are expected to be clinically irrelevant when nontargeted major coronary arteries are not closely situated to the targeted vessel segment.

Both biplane angiography and MSCT allow definition of the coronary artery STV during the cardiac cycle as a relatively small potential target volume for CRT. The most challenging technical obstacle in studying the feasibility of CRT for the treatment of coronary artery in-stent restenosis thereby is overcome. However, the use of radiotherapy for the afore-mentioned purpose has been reduced substantially because new treatment techniques have emerged.

The described imaging strategies to account for cardiac motion can be applied for any thoracic or upper abdominal target volume.

MSCT to determine and incorporate respiratory target volume motion

Chapter 6 reports on a study of patients with lung tumors who were scanned using 4D respiratory-gated MSCT. For each patient 10 MSCT datasets equally distributed throughout consecutive respiratory cycles were retrospectively reconstructed from the acquired MSCT data. The maximum amplitude of the lung tumor center of mass displacements throughout the respiratory cycle was 2.2 ± 1.0 (mean \pm standard deviation) mm in the lateral direction, 3.3 ± 1.4 mm in the ventrodorsal direction and 13.3 ± 7.4 mm in the craniocaudal direction. **Chapter 7** describes a comparison between a generalized 3D and an individualized 4D MSCT imaging strategy to account for respiratory lung tumor motion. A geometrical discrepancy between the former and latter strategy was found. Individualized determination of respiratory lung tumor motion by 4D respiratory-gated MSCT represents a better and simple strategy to incorporate periodic physiological motion compared to a generalized approach. The 4D MSCT technique to account for respiratory motion can be applied for any thoracic or abdominal target volume.

The studies in this thesis mainly focus on the advantages for CRT of 4D MSCT gated to periodic physiological motion. Target volumes affected by respiratory and cardiac motion can benefit the most from this imaging strategy. Moreover, 4D MSCT gated to periodic physiological motion can also be useful for novel

treatment techniques such as gated, tumor tracking and breath holding CRT. Four-dimensional imaging by MSCT can therefore improve routine and state-of-the-art clinical practice in radiotherapy. Future studies on the use of 4D MSCT in CRT should include exploration of the combination with other imaging modalities such as magnetic resonance imaging, and on efficient strategies to facilitate treatment planning using 4D imaging datasets.

Samenvatting en conclusies

Conformatieradiotherapie is een vorm van uitwendige radiotherapie. Deze behandeltechniek beoogt nauwkeurige bestraling van het doelvolumen, terwijl gezonde omliggende weefsels en organen zoveel mogelijk worden ontzien. Hiertoe wordt tijdens de voorbereiding van conformatieradiotherapie met behulp van een computertomografie (CT) scanner de driedimensionale omvang en ligging van het doelvolumen bepaald. Door technische ontwikkelingen wordt conformatieradiotherapie steeds nauwkeuriger toegepast. Hierdoor wordt het toenemend belangrijk om rekening te houden met factoren die de behandelnaauwkeurigheid kunnen beïnvloeden. Voorbeelden van deze factoren zijn de ademhaling en hartslag en kleine verplaatsingen van de patiënt tijdens de bestraling.

In de regel wordt de totale stralingsdosis over een aantal dagen verdeeld in zogenoemde fracties. Zo'n bestralingsfractie duurt doorgaans enkele minuten. Tijdens de bestraling van doelvolumina in de borstholte en buik beïnvloeden met name de ademhaling en hartslag de nauwkeurigheid van de behandeling. Het is gebruikelijk dat de patiënt doorademt tijdens een bestralingsfractie. Een bestralingsplan gebaseerd op een enkele conventionele CT scan van een doelvolumen in de borstholte of buik, houdt daarom geen rekening met de invloed van de ademhaling en hartslag. Tijdens de gangbare toepassing van conformatieradiotherapie wordt deze beperking gecompenseerd door voor iedere patiënt het betreffende doelvolumen uit te breiden met een vaste driedimensionale marge. Deze marge is empirisch bepaald en niet afgestemd op de individuele patiënt. Hierdoor is de kans groot dat het doelvolumen te weinig stralingsdosis ontvangt en de omliggende gezonde weefsels en organen juist teveel.

In dit proefschrift worden geavanceerde beeldvormingsstrategieën beschreven waarmee voor iedere patiënt individueel de invloed van de ademhaling en hartslag kan worden bepaald en geïntegreerd in het doelvolumen. Met deze strategieën is het mogelijk voor iedere patiënt individueel, nauwkeurig rekening te houden met de vierde dimensie. Namelijk de invloed van tijd op de positie van het doelvolumen tijdens de bestralingsfractie.

Vierdimensionale röntgendoorlichting voor de bepaling en integratie van door de hartslag veroorzaakte doelvolumebewegelijkheid

Een dotterbehandeling komt in aanmerking bij pijnklachten door een vernauwing in de kransslagader. Helaas komt binnen enkele weken of maanden in een derde van de geslaagde behandelingen de vernauwing terug. Deze hervernauwing noemt men restenose. Plaatsing van een conventionele stent in de kransslagader vermindert de kans op restenose enigszins. Een stent is een metalen veertje dat in de kransslagader kan worden gebracht om het bloedvat open te helpen houden. Nieuwe behandelingsmethoden zijn ontwikkeld om de kans op restenose nog verder te verminderen.

Eén van deze nieuwe ontwikkelingen is het bestralen van de plaats van de dotterbehandeling met een speciale catheter die een inwendige stralingsbron bevat. Deze behandeltechniek wordt intravasculaire brachytherapie genoemd. Intravasculaire brachytherapie is een effectieve therapie om restenose aanzienlijk te beperken. Deze invasieve, inwendige vorm van radiotherapie heeft echter een aantal nadelen die in mindere mate gelden voor uitwendige radiotherapie. De laatstgenoemde behandelwijze maakt het bijvoorbeeld mogelijk de dosis te fractioneren, terwijl dit met brachytherapie geen reële optie is. Een studie naar de technische haalbaarheid van uitwendige radiotherapie ter behandeling van restenose in kransslagaderstents, vormde een geschikt model binnen de doelstelling van dit proefschrift. In **hoofdstuk 2** wordt aangetoond dat met hartfilm-gecorrleerde vierdimensionale röntgendoorlichtingsbeelden, de door de hartslag veroorzaakte beweeglijkheid van het doelvolumen nauwkeurig kan worden bepaald. Deze beweeglijkheid is geïntegreerd tot het door de stent doorkruiste volume onder invloed van de hartslag. Dit door de stent doorkruiste volume vormde minder dan 0.8% van het gehele hartvolume en kan hiermee worden beschouwd als een potentieel doelvolumen voor uitwendige radiotherapie. In **hoofdstuk 3** wordt beschreven dat een dergelijk door de stent doorkruist volume significant kan worden gereduceerd wanneer het wordt bepaald tijdens een deel van de hartslag.

Omdat vierdimensionale röntgendoorlichtingsbeelden niet rechtstreeks gebruikt kunnen worden voor een bestralingsplan, is getracht de beschreven strategie met behulp van een geavanceerde CT-scanner te verrichten.

Multislice spiraal computertomografie voor de bepaling en integratie van door de hartslag veroorzaakte doelvolumenbeweeglijkheid

De röntgenbron en het detectorsysteem in het type CT scanners geïnstalleerd op de meeste radiotherapieafdelingen, draaien continu rondom de patiënt waarbij coupe voor coupe wordt gescand. Door de te lange beeldacquisitietijden zijn deze scanners niet geschikt voor het bepalen van de invloed van de ademhaling en hartslag op de beweeglijkheid van doelvolumina in de borstholte en buik. Met de introductie van zogenoemde multislice spiraal computertomografie (MSCT) scanners is dit wel mogelijk geworden. Met deze techniek kunnen namelijk meerdere coupes tegelijk gescand worden en kan sneller gescand worden. In **hoofdstuk 4** wordt aangetoond dat de door de hartslag veroorzaakte variatie in de driedimensionale positie van kransslagaderstents, kan worden bepaald met vierdimensionale MSCT. Hiertoe is de hartfilm-gecorrleerde beeldvormingsinformatie behorende bij 10 gelijk over de hartcyclus verdeelde fasen retrospectief geselecteerd. Vervolgens is tijdens de verschillende fasen de corresponderende driedimensionale positie van de stent bepaald. Integratie van deze stentposities vormde een maat voor het door de stent

doorkruiste volume onder invloed van de hartslag. Dit potentiële doelvolume voor conformatieradiotherapie vormde minder dan 0.6% van het gehele hartvolume van de onderzochte patiënten. In **hoofdstuk 5** worden de dosimetrische verschillen beschreven tussen een inwendig bestralingsplan gericht op een kransslagaderstent en een uitwendig bestralingsplan gericht op een doelvolume als beschreven in hoofdstuk 4. Weliswaar bleken de doses in het hart met uitwendige radiotherapie hoger, maar naar verwachting niet zodanig dat sprake is van klinische relevantie.

Met zowel röntgendoorlichtingsbeelden als MSCT scans is het mogelijk gebleken de door de hartslag van patiënten veroorzaakte beweeglijkheid van kransslagaderstents te bepalen. Het tijdens de hartcyclus door de stent doorkruiste volume is een integratie van deze beweeglijkheid en vormt een relatief klein potentieel doelvolume. Uitwendige radiotherapie ter behandeling van restenose in kransslagaderstents kan hierdoor technisch haalbaar worden geacht. Echter, het gebruik van radiotherapie voor de genoemde toepassing is sterk afgenomen vanwege nieuwe behandel mogelijkheden.

De beschreven beeldvormingsstrategieën zijn toepasbaar voor ieder onder invloed van de hartslag beweeglijk doelvolume in de borstholte en bovenbuik.

Multislice spiraal computertomografie voor de bepaling en integratie van door de ademhaling veroorzaakte doelvolumebeweeglijkheid

Hoofdstuk 6 beschrijft een studie van patiënten met longtumoren. Met vierdimensionale MSCT scans, retrospectief gecorreleerd met 10 over de ademhalingscyclus gelijk verdeelde fasen, is de beweeglijkheid van longtumoren bepaald. De gemiddelde maximale uitslag van de tumor, veroorzaakt door de ademhaling, was 13.3 mm (standaard deviatie [SD] 7.4 mm) in de lengterichting van de patiënt, 3.3 mm (SD 1.4 mm) in de voorachterwaartse richting en 2.2 mm (SD 1.0 mm) in de zijwaartse richting. **Hoofdstuk 7** beschrijft een studie waarin beeldvorming met conventionele CT scans tijdens de voorbereiding van gangbare conformatieradiotherapie, wordt vergeleken met de als in hoofdstuk 6 beschreven vierdimensionale beeldvorming met MSCT scans. De gangbare methode betrof uitbreiding van de longtumorposities met een empirische marge. De vierdimensionale methode betrof integratie van de bepaalde beweeglijkheid tot het door de longtumor doorkruiste volume tijdens de ademhalingscyclus. Beeldvorming volgens de gangbare praktijk resulteerde in een significant groter doelvolume dan het door de longtumor doorkruiste volume onder invloed van de ademhaling. Eerstgenoemd doelvolume overlapte laatstgenoemd doelvolume geheel of gedeeltelijk. Vergeleken met de gangbare praktijk in de conformatieradiotherapie is vierdimensionale beeldvorming een

betere basis voor precisiebestraling. Het is toepasbaar voor ieder onder invloed van de ademhaling beweeglijk doelvolumen in de borstholte en buik.

De studies in dit proefschrift richten zich met name op de voordelen van retrospectief met de ademhaling of hartslag gecorreleerde vierdimensionale MSCT binnen de conformatieradiotherapie. De beschreven technieken zijn vooral toepasbaar bij patiënten met doelvolumina die onder invloed van de genoemde fysiologische effecten beweeglijkheid tonen. Tevens kan vierdimensionale MSCT van nut zijn voor andere nieuwe behandelingstechnieken zoals “triggered”, “tumor tracking” en “breath holding” conformatieradiotherapie. Toekomstige studies dienen zich te richten op methoden waarmee de voordelen van deze beeldvormingstechniek kunnen worden geoptimaliseerd voor radiotherapeutische toepassingen: gecombineerd gebruik met andere beeldvormingstechnieken, zoals MRI-scans. En efficiënte strategieën om vierdimensionale beeldvormingsinformatie te verwerken tijdens het vervaardigen van een bestralingsplan.

Dankwoord

Allereerst wil ik de leden van de kleine commissie bedanken voor het beoordelen van dit proefschrift.

Zeer veel dank ben ik verschuldigd aan mijn promotor prof. dr. P.C. Levendag. Beste Peter, dankzij de door jou gecreëerde mogelijkheden heb ik mijn onderzoek kunnen doen. Jouw basisidee en motiverende begeleiding zijn essentieel geweest voor mijn onderzoek. Niet alleen op het professionele vlak, maar ook op het persoonlijke vlak kijk ik met veel genoegen terug op mijn onderzoeksperiode.

Zeer veel dank ben ik ook verschuldigd aan mijn copromotor dr. P.J.C.M. Nowak. Beste Peter, als “fusie” van een fysicus en radiotherapeut-oncoloog was je een ideale tweede begeleider van mijn onderzoek. Dagelijks mocht ik je bestoken met mijn vragen en ideeën. Mijn onderzoek had ik niet kunnen verrichten zonder de door jou geschreven software.

Prof. dr. P.W. Serruys, beste Patrick, zeer bedankt voor de gelegenheid om binnen jouw afdelingssectie een deel van mijn onderzoek te verrichten. En voor jouw adviezen en commentaar op mijn publicaties.

Koen Nieman, ik heb mogen profiteren van jouw pionierswerk op het gebied van multislice CT. Mijn dank gaat uit naar jou, prof. dr. P.J. de Feijter en Aristoteles Munne.

Veel dank ben ik verschuldigd aan dr. ir. C.J. Slager, ing. J.C.H. Schuurbijs en dr. ir. J.J. Wentzel. Beste Kees, Hans en Jolanda, in een gastvrije omgeving heb ik gebruikmakend van de door jullie ontwikkelde technieken binnen relatief korte tijd voor mij waardevol onderzoek verricht. Er was altijd tijd voor vragen en discussie. Ik heb veel van jullie geleerd.

Dr. S.G. Carlier, beste Stéphane, bedankt voor jouw adviezen en jouw commentaar op enkele van mijn publicaties.

Filippo Cademartiri, I've enjoyed our pleasant cooperation for respiratory-gated CT. Thank you for the important and instructive radiological input. Prof. dr. P.M.T. Pattynama, bedankt voor de mogelijkheden die mij zijn geboden op de afdeling radiologie en voor uw commentaar op mijn publicaties. Verder dank ik van de afdeling Radiologie Henri Vrooman, de laboranten en baliemedewerkers.

Thomas Flohr, thank you for all the essential custom-made solutions with regard to respiratory-gated CT. Many thanks also to others at Siemens Medical Solutions in Forchheim who were involved with this project.

Harold Smeets van Viasys Healthcare, bedankt voor de hardware- en softwarematige ondersteuning op het gebied van spirometrie. Henk Stam, bedankt voor jouw longfysiologische adviezen en jouw commentaar op mijn publicaties.

Alle artsen van de afdeling interne-oncologie en interne-endocrinologie, bedankt voor de medewerking die is verleend aan mijn onderzoek.

Wijlen Jan Nanninga, Gerry van Oortmarssen en Peter Schoor van Elekta Oncology Systems, dank voor jullie steun en betrokkenheid. Jörn Wulf, Ulrich Hädinger and prof. M. Flentje, thank you for introducing me and Peter Nowak with the practical principles of extracranial stereotactic radiotherapy. Prof. dr. J.N. IJzermans en dr. C.H. van Eijck, bedankt voor jullie belangrijke bijdrage aan het opzetten van extracraniële stereotactische radiotherapie.

Hans Kneefel, Hans Vuik en Aad Moerman, dank voor jullie hulp op (foto)grafisch gebied. Mevrouw M. Westerhout en de heer drs. Volkers, dank voor jullie hulp bij het verzamelen dan wel verwerken van literatuur.

Ik dank alle medewerkers van de afdeling Radiotherapie-Centrumlocatie voor de prettige werksfeer. Een aantal personen wil ik in het bijzonder bedanken. Allereerst “mijn” secretaresses Wonny Venloo, Astrid Mertens en Sevcan Tas. Verder mijn “lunchbroeders” Nico van Gulik, Hans Zandbergen, Rolf Pais en Edwin Sluijter. Connie de Pan, bedankt voor het maken van de bestralingsplannen en DVH's. Alle andere stereotaxielaboranten, bedankt voor jullie praktische hulp en jullie begrip als ik weer eens in de weg zat.

Uiteraard dank ik ook alle andere medewerkers van de gehele afdeling radiotherapie, waarvan ik er een aantal wil noemen. Namelijk Hans Joosten, Bart Kanis, Hafid Akhiat, Edward Donkersloot, Peter van Ravensberg, Jeannette Schilperoord, alle laboranten en andere medewerkers die betrokken zijn geweest bij de eerste schreden op het pad van de extracraniële stereotaxie, de arts-assistenten en radiotherapeuten-oncologen. Hans Marijnissen, bedankt voor jouw fysische bijdrage aan een van mijn artikelen. Ben Heijmen, bedankt voor jouw commentaar op delen van dit proefschrift.

Het was voor mij een moeilijke beslissing om te bepalen hoe ik mijn weg zou vervolgen binnen de oncologie. Uiteindelijk zag ik af van de opleidingsplaats radiotherapie en heb ik gekozen voor de klinische genetica. Dr. F.H. Menko, bedankt voor de adviezen. Prof. dr. L.P. ten Kate, bedankt voor de opleidingsplaats klinische genetica.

Mijn zuster en Ralph Akrum, bedankt voor jullie inspanningen als paranimf.

Mijn grootste dank gaat uit naar mijn familie. Rudi, Patricia, Ron, Christina, Djair, Daniel, Diana, Isaura, pa en – last but not least – ma, bedankt voor jullie belangrijke steun.

List of publications

1. Leter EM, Levendag PC, Nieman K, Slager CJ, Carlier SG, Serruys PW, Nowak PJ. Comparison of different methods to define a target volume for external beam radiation therapy of restenotic coronary arteries. *Cardiovasc Radiat Med* 2001;2:208-212.
2. Coen VLMA, Leter EM, Levendag PC. Late effects of ionizing radiation exposure. In: Tripuraneni P, Jani SK, Minar E, Leon MB, editors. Intravascular brachytherapy. From theory to practice. London: Remedica Publishing Limited. 2001;27-39.
3. Leter EM, Nowak PJ, Nieman K, de Feijter PJ, Carlier SG, Munne A, Serruys PW, Levendag PC. Definition of a moving gross target volume for stereotactic radiation therapy of stented coronary arteries. *Int J Radiat Oncol Biol Phys* 2002;52:560-565.
4. Leter EM, Schuurbiens JCH, Levendag PC, Nowak PJCM, Wentzel JJ, Carlier SG, Serruys PW, De Feijter PJ, Slager CJ. Coronary stent traversed volume during the cardiac cycle defined as a target for high-precision radiotherapy by using biplane angiograms. *Radiother Oncol* 2002;63:103-106.
5. Leter EM, Nowak PJ, Nieman K, Marijnissen JP, Carlier SG, de Pan C, Serruys PW, Levendag PC. Dosimetric comparison between high-precision external beam radiotherapy and endovascular brachytherapy for coronary artery in-stent restenosis. *Int J Radiat Oncol Biol Phys* 2002;54:1252-1258.
6. Leter EM, Schuurbiens JCH, Nowak PJCM, Levendag PC, Wentzel JJ, Pattynama PMT, De Feijter PJ, Serruys PW, Slager CJ. A biplane angiographic study on cardiac motion of coronary artery stents: Options to minimize the target volume for high-precision external beam radiotherapy of coronary artery in-stent restenosis. *Int J Radiat Oncol Biol Phys* 2004;58:278-283.

Curriculum vitae

De auteur van dit proefschrift werd op 5 april 1971 geboren te Haarlem. Na het behalen van het VWO diploma in 1989 aan het categoriaal atheneum College Hageveld in Heemstede, wijdde hij een jaar aan sportbeoefening. In 1990 startte hij met de studie Biomedische Wetenschappen aan de Rijksuniversiteit te Leiden. In 1991 maakte hij een overstap naar de studie Geneeskunde aan dezelfde universiteit. Na het behalen van het artsexamen in december 1997 werkte hij een korte periode als zaalarts neurologie in het Ziekenhuis Leyenburg en het Medisch Centrum Haaglanden te Den Haag. Vanaf september 1998 werkte hij ruim een jaar als AGNIO klinische genetica in het VU medisch centrum te Amsterdam. Vanaf november 1999 werkte hij als arts-onderzoeker op de afdeling Radiotherapie in het Erasmus Medisch Centrum te Rotterdam, hetgeen resulteerde in dit proefschrift. In juni 2003 ving hij aan met de opleiding tot klinisch geneticus in het VU medisch centrum te Amsterdam (opleider prof. dr. L.P. ten Kate), met familiale tumoren als beoogd aandachtsgebied.

Financial support for the publication of this thesis was provided by:

Siemens Medical Solutions

Radionics

Elekta Oncology Systems

